REPORT DOCUMENTATION PAGE

AFRL-SR-AR-TR-02-

0226

1. AGENCY USE ONLY *(Leave blank)*	2. REPORT DATE	3. REPORT TYPE AND DATES COVERED
		01 Dec 98 - 28 Feb 02

4. TITLE AND SUBTITLE
High Order Methods for the Numerical simulations of Reactive High Speed Flows

5. FUNDING NUMBERS
F49620-99-1-0077

6. AUTHOR(S)
David Gottlieb

7. PERFORMING ORGANIZATION NAME(S) AND ADDRESS(ES)
Brown University
Box 1929
164 Angell Street
Providence RI 02912

8. PERFORMING ORGANIZATION REPORT NUMBER

9. SPONSORING/MONITORING AGENCY NAME(S) AND ADDRESS(ES)
AFOSR/NM
801 N. Randolph Street Room 732
Arlington, VA 22203-1977

10. SPONSORING/MONITORING AGENCY REPORT NUMBER
F49620-99-1-0077

11. SUPPLEMENTARY NOTES

12a. DISTRIBUTION AVAILABILITY STATEMENT
APPROVED FOR PUBLIC RELEASE, DISTRIBUTION UNLIMITED

12b. DISTRIBUTION CODE

13. ABSTRACT *(Maximum 200 words)*

The goal of this research was to study the computational issues involved in constructing an accurate, efficient and flexible computational framework for the modeling of supersonics reactive flows, and to apply the methods thus developed to problems originated from the Air-Force labs. The main components of this framework are: High order accuracy numerical methods are applied in order to resolve the important detailed fearures of the flow. Spectral multidomain methods. Weighted Essentially Non Oscillatory (WENO) methods. High Order compact finite difference schemes. Domain decomposition techniques are used, the methods are based on penalty impositions of interface bundary conditions in a proven timetable way. The discontinuous Galerkin methodology is implemented in the finite differences component of the research. Structured as well as unstructured grid multi-domain spectral methods are being developed. In the structured grid methods the building blocks are cubes (in 3D) or rectangles (in 2D). The grid is predefined by a tensor product of Gaussian points to assure spectral accuracy. The standard building blocks in the unstructured grid methods are the tetrahedral elements (in 3D) or triangles (in 2D) with a newley developed unstructured nodal basis within each element.

14. SUBJECT TERMS

15. NUMBER OF PAGES
34

16. PRICE CODE

17. SECURITY CLASSIFICATION OF REPORT	18. SECURITY CLASSIFICATION OF THIS PAGE	19. SECURITY CLASSIFICATION OF ABSTRACT	20. LIMITATION OF ABSTRACT

May 2002

Final Tech

High Order Methods for the Numerical Simulations of Reactive High Speed Flows

AFOSR Grant AF49620-99-1-0077

David Gottlieb, Chi Wang Shu, Wai Sun Don, Jan Hesthaven
Division of Applied Mathematics, Brown University

1 Introduction

The goal of this research was to study the computational issues involve in constructing an accurate, efficient and flexible computational framework for the modeling of supersonics reactive flows, and to apply the methods thus developed to problems originated from the Air-Force labs.

The main components of this framework are:

- High order accuracy numerical methods are applied in order to resolve the important detailed features of the flow.
  - Spectral multidomain methods.
  - Weighted Essentially Non Oscillatory (WENO) methods.
  - High Order compact finite difference schemes.
- Domain decomposition techniques are used,
  - The methods are based on penalty impositions of interface boundary conditions in a proven time-stable way. The discontinuous Galerkin methodology is implemented in the finite differences component of the research.
- Structured as well as unstructured grid multi-domain spectral methods are being developed.
  - In the structured grid methods the building blocks are cubes (in 3D) or rectangles (in 2D). The grid is predefined by a tensor product of Gaussian points to assure spectral accuracy.
  - The standard building blocks in the unstructured grid methods are the tetrahedral elements (in 3D) or triangles (in 2D) with a newly developed unstructured nodal basis within each element.
- To stabilize the spectral and the compact schemes:
  - Superviscosity terms are used to stabilize the methods in the presence of shock waves. To minimize the amount of added work, the superviscosity method is carried out in a form of a low pass exponential filter.
  - Post-processing, aimed at removing the Gibbs phenomenon, is applied to recover spectral accuracy.
- Far field boundary conditions to eliminate non-physical reflections from the boundaries of the computational domain, are applied.

The methods thus developed are being currently applied to the simulations of recessed cavity flameholders and to the study of mixing and instabilities induced by shock waves.

In the following we will review past accomplishments and future tasks to be performed. It composed of the following Sections:

- Spectral methods for discontinuous problems.
- Recessed cavity flameholders
- Weighted Essentially Non-Oscillatory (WENO) schemes.
- Spectral multi-domain methods.
- Unstructured grid based spectral and WENO methods.
- Far field boundary conditions for the Euler equations of Gas Dynamics.

2 Spectral Methods for Shock Waves

The use of spectral and other high order accuracy methods for the simulation of high Mach number flows has been one of the main topics of this research. Spectral methods, due to their accuracy, resolve small scale phenomena better than lower order methods and therefore they are the methods of choice when long time integrations are performed and fine details of the flow are needed. The presence of large gradients, however, poses difficulties in the application of spectral methods both on the theoretical and the practical level. We would like to describe the state of the art in the application of spectral methods to discontinuous problems. First, we will briefly review the main components of the spectral shock capturing techniques, and will list the proposed research topics in this area. We then will give a more detailed review of the achievements in the field.

The main components of a spectral shock capturing techniques are

- Spectral viscosity terms are added to stabilize the schemes. The following methods are currently being used:
  - Spectral viscosity, where the viscosity is added only to the high modes of the equation.
  - Spectral super viscosity. Here a high term derivative is added to stabilize the equation without changing the order.
  - A low pass filter, equivalent to the Spectral Super Viscosity is added.
- At the end of the calculation the discontinuities are located. There are several methods of accomplishing that.
  - Methods based on decay rate of the coefficients.
  - Methods based on conjugate sums.
  - Wavelet based methods.
- Reconstruction of the solution, based on the resolution of the Gibbs phenomenon is carried out.

There are many practical problems in the above outlined framework that need to be addressed.

- What is the best mechanism for stabilizing the spectral scheme? This is a very important question that has a far reaching impact on the successful simulations of reactive flow. We propose to study the interplay between stability and accuracy and to find the optimal way of stabilizing the spectral scheme. We will study the spectral stabilizers in the context of real life applications.
- The reconstruction step is supported by a solid theoretical foundation, however its application is still more an art than science in the sense that there are too many free parameters that are crucial to the success of the method. We propose to study the role of those free parameters in order to come with automatic post processing step.

The application of spectral methods to flows containing shock waves has been extensively studied by us and others in the past and significant advances had been made. We briefly summarize the current state of the research.

2.1 Approximation Theory

2.1.1 Enhanced Convergence by the Use of Filters

One manifestation of the slow and nonuniform convergence of the spectral approximation $\mathcal{I}_N u$ of a piecewise smooth function u is found in the linear decay of the global expansion coefficients, $\tilde{u}_n$. This realization also suggests that one could attempt to modify the global expansion coefficients to enhance the convergence rate of the spectral approximation. The critical question to address naturally becomes exactly how one should modify the expansion to ensure enhanced convergence to the correct solution.

Let us consider the filtered approximation, $\mathcal{F}_N u_N(x)$, of the form

$$\mathcal{F}_N u_N(x) = \sum_{n=-N}^{N} \sigma\left(\frac{n}{N}\right) \tilde{u}_n \exp(inx) \ , \tag{2.1}$$

where $\tilde{u}_n$ signifies the discrete expansion coefficients of $u_N(x,t)$ and $\sigma(\eta)$ is a real filter function with the following properties

$$\sigma(\eta) = \begin{cases} \sigma(-\eta) \\ \sigma(0) = 1 \\ \sigma^{(q)}(0) = 0 \quad 1 \le q \le 2p-1 \\ \sigma(\eta) = 0 \qquad |\eta| \ge 1 \end{cases} . \tag{2.2}$$

If $\sigma(\eta)$ has at least $2p-1$ continuous derivatives, $\sigma(\eta)$ is termed a filter of order $2p$.

As the filter is nothing more than a low pass filter, it is not surprising that the filtered function converges faster than the unfiltered original expansion. To understand exactly how much the filtering modifies the convergence rate, let us assume that $u(x)$ is piecewise $C^{2p}[0,2\pi]$ with one discontinuity located at $x = \xi$. Let us furthermore assume that the filter is of order $2p$. Then the pointwise error of the filtered approximation is given as

$$|u(x) - \mathcal{F}_N u_N(x)| \le C \frac{1}{N^{2p-1} d(x,\xi)^{2p-1}} K(u) + C \frac{\sqrt{N}}{N^{2p}} \|u^{(2p)}\|_{L^2_B[0,2\pi]} ,$$

where $d(x,\xi)$ measures the distance from x to the point of discontinuity, ξ, $K(u)$ is uniformly bounded away from the discontinuity and a function of $u(x)$ only. Also $\|\cdot\|_{L^2_B[0,2\pi]}$ signifies the broken $L_2[0,2\pi]$-norm.

While the details of the proof of this result are quite technical the interpretation of the result is simple, and perhaps somewhat surprising. It states the convergence rate of the filtered approximation is determined solely by the the order, $2p$, of the filter, $\sigma(\eta)$, and the regularity of the function, $u(x)$, away from the point of discontinuity. In particular, if the function, $u(x)$, is piecewise analytic and the order of the filter increases with N, one recovers an exponentially accurate approximation to the unfiltered function everywhere except very close to the discontinuity.

The actual choice of the filter function, $\sigma(\eta)$, is one of great variety and numerous alternatives are discussed in the literature. A particularly popular one is the exponential filter

$$\sigma(\eta) = \exp\left(-\alpha \eta^{2p}\right) ,$$

which satisfies all the conditions in Eq.(2.2) except that of being zero for $|\eta| \ge 1$. However, by choosing $\alpha = -\ln \varepsilon_M$, with ε_M representing the machine accuracy, $\sigma(\eta)$ vanishes for all practical purposes when $|\eta|$ exceeds one and the exponential filter allows for the recovery of a piecewise exponentially accurate approximation of a piecewise analytic function away from the point of discontinuity.

When applying the filter it is worth noticing that, as for differentiation, the spectral filtering, has a dual formulation, expressed as a matrix operation, of the form

$$\mathcal{F}_N u_N(x_i) = \sum_{j=0}^{2N-1} \mathrm{F}_{ij} u_N(x_j) , \quad \mathrm{F}_{ij} = \frac{1}{N} \sum_{n=0}^{N} \frac{1}{c_n} \sigma\left(\frac{n}{N}\right) \cos(n(x_i - x_j)) ,$$

where $c_0 = c_N = 2$ and $c_n = 1$ otherwise.

The use of a filter in a Chebyshev collocation method is similar to that of the Fourier approximation, i.e., it can be expressed as

$$\mathcal{F}_N u_N(x) = \sum_{n=0}^{N} \sigma\left(\frac{n}{N}\right) \tilde{u}_n T_n(x) ,$$

or on its dual form

$$\mathcal{F}_N u_N(x_i) = \sum_{j=0}^{N} \mathrm{F}_{ij} u_N(x_j) , \quad \mathrm{F}_{ij} = \frac{2}{N c_j} \sum_{n=0}^{N} \frac{1}{c_n} \sigma\left(\frac{n}{N}\right) T_n(x_i) T_n(x_j) .$$

While the use of spectral filtering as discussed in the above remains the most popular way of enhancing the convergence rate, an alternative approach can be realized by observing that the Gibbs phenomenon is also a manifestation of the global nature of the interpolating polynomial. In other words, one could attempt to improve on the quality of the approximation by localizing the approximation close to the point of the discontinuity.

This approach, known as physical space filtering, operates directly on the interpolating polynomials rather than the expansion coefficients. To illustrate the basic idea consider the filtered Fourier approximation

$$\mathcal{F}_N u_N(x) = \sum_{j=0}^{2N-1} u(x_j) l_j^\sigma(x) \ ,$$

where x_j are the usual equidistant grid and the filtered Lagrange interpolation polynomial takes the form

$$l_j^\sigma(x) = \frac{1}{2N} \sum_{n=-N}^{N} \sigma\left(\frac{n}{N}\right) \frac{1}{\bar{c}_n} \exp\left(in(x - x_j)\right) \ .$$

Clearly, if $\sigma(\eta) = 1$ we recover the Fourier interpolation polynomial. However, we do not need to maintain the close connection to the trigonometric interpolation polynomials, as expressed in $l_j^\sigma(x)$, but can choose to use any reasonable kernel, $\psi(y, x)$, that approximates a delta function as $y - x$ approaches zero. We can exemplify this idea by considering

$$\psi(y, x) = \rho(\xi(y, x)) \frac{1}{2\varepsilon} \sum_{n=-N}^{N} \exp(in\xi(y, x)) \ ,$$

where

$$\xi(y, x) = \frac{x - y}{\varepsilon} \ .$$

We assume that $u(x) \in C^{2p}[y - \varepsilon, y + \varepsilon]$ and $\rho(\xi(y, x))$ controls the amounts of localization as

$$\rho(0) = 1 \ , \rho(\xi(y, x)) = 0 \quad \text{for } |\xi(y, x)| \geq 1 \ ,$$

i.e., the kernel vanished outside of the symmetric interval $[y - \varepsilon, y + \varepsilon]$. Note also that $\frac{1}{2\varepsilon} \sum_{n=-N}^{N} \exp(in\xi(y, x))$ is an approximation to a y-centered delta function. It this setting it had been shown that the order of the filter and the regularity of the function away from the point of discontinuity solely determines the convergence rate of the filtered approximation. Exponential convergence can be recovered everywhere except very close to the point of discontinuity as measured through ε. The need to specify the size, ε, of the symmetric interval remains a practical obstacle to the use of the physical space filters.

While the use of filters can have a dramatic impact on the quality of the convergence of a global approximation to a discontinuous function, such techniques are unable to improve on the quality of the approximation as one approaches the point of discontinuity. Moreover, filtering generally treats the Gibbs oscillations as a source of noise and attempts to remove it. However, as has been speculated in the past and recently shown rigorously, the Gibbs oscillations are not noise but rather contain sufficient information to reconstruct an exponentially convergent approximation everywhere provided only that the location of the discontinuity is known, i.e., the Gibbs phenomenon can be overcome completely.

2.1.2 Resolving the Gibbs Phenomenon

In the following we outline the key elements of a general theory that establishes the possibility of recovering a piecewise exponentially convergent series to a piecewise analytic function, $u(x) \in L_w^2[-1, 1]$, having knowledge of the global expansion coefficients and the position of the discontinuities only.

The basic element of this new approach is the identification of a new basis with very special properties and, subsequently, the expansion of the slowly convergent truncated global expansion in this new basis. Provided this new basis satisfies certain conditions, the new expansion has the remarkable property that it is exponentially convergent to the original piecewise analytic function even though it uses information from the slowly convergent global expansion.

As previously we assume that

$$\mathcal{P}_N u(x) = \sum_{n=0}^{N} \hat{u}_n \phi_n(x) \ , \ \hat{u}_n = \frac{1}{\gamma_n} (u, \phi_n)_w \ ,$$

with $\gamma_n = \|\phi_n\|_w^2$. Note in particular that this also contains the Fourier case provided

$$\phi_n(x) = \exp\left[i\left(n - \frac{N}{2}\right)\pi x\right] \ .$$

Let us also assume that there exists an interval $[a,b] \subset [-1,1]$ in which $u(x)$ is analytic and, furthermore, that the original truncated expansion is pointwise convergent in all of $[-1,1]$ with the exception of a finite number of points. We shall introduce the scaled variable

$$\xi(x) = -1 + 2\frac{x-a}{b-a} \ .$$

Clearly, $\xi : [a,b] \to [-1,1]$.

We define a new basis, $\psi_n^\lambda(\xi)$, which is orthogonal in the weighted inner product, $(\cdot,\cdot)_w^\lambda$ where λ signifies that the weight, $w(x)$, may depend on λ, i.e.,

$$\left(\psi_k^\lambda, \psi_n^\lambda\right)_w^\lambda = \|\psi_n^\lambda\|^2_{L^2_w[-1,1]}\delta_{kn} = \gamma_n^\lambda \delta_{kn} \ .$$

Furthermore, we require that if $v(\xi)$ is analytic then

$$\mathcal{P}_\lambda v(\xi) = \sum_{n=0}^{\lambda} \frac{1}{\gamma_n^\lambda}\left(v, \psi_n^\lambda\right)_w^\lambda \psi_n^\lambda(\xi) \ ,$$

is pointwise exponentially convergent as λ increases, i.e.,

$$\|v - \mathcal{P}_\lambda v\|_{L^\infty[-1,1]} \leq Ce^{-c\lambda} \ ,$$

with $c > 0$.

A final condition, however, sets this basis apart and is central in order to overcome the Gibbs phenomenon. We shall require that there exists a number $\beta < 1$, such that for $\lambda = \beta N$ we have

$$\left|\frac{1}{\gamma_n^\lambda}\left(\phi_k(x(\xi)), \psi_n^\lambda(\xi)\right)_w^\lambda\right| \|\psi_n^\lambda\|_{L^\infty[-1,1]} \leq \left(\frac{\alpha N}{k}\right)^\lambda \ , \tag{2.3}$$

for $k > N$, $n \leq \lambda$ and $\alpha < 1$. The interpretation of this condition is that the projection of the high modes of ϕ_k onto the basis, ψ_n^λ, is exponentially small in the interval, $\xi \in [-1,1]$. In other words, by reexpanding the slowly decaying ϕ_k-based global expansion in the local ψ_n^λ-basis an exponentially accurate local approximation is recovered. Moreover, this can be achieved everywhere in the domain where $u(x)$ is analytic. We shall term this latter, and crucial, condition on ψ_n^λ the Gibbs condition to emphasize its close connection to the resolution of the Gibbs phenomenon.

Provided only that the ψ_n^λ-basis, which we term the Gibbs complementary basis, is complete we recover the key result

$$\left\| u(x) - \sum_{n=0}^{\lambda} \frac{1}{\gamma_n^\lambda}\left(\mathcal{P}_N u, \psi_n^\lambda\right)_w^\lambda \psi_n^\lambda(\xi(x))\right\|_{L^\infty[a,b]} \leq C\exp(-cN) \ ,$$

where $\lambda = \beta N$ and $u(x)$ is analytic in the interval $[a,b]$.

In other words, if a Gibbs complementary basis exists it is possible to reconstruct a piecewise exponentially convergent approximation to a piecewise analytic function from the information contained in the original very slowly converging global approximation using only knowledge about the location of the points of discontinuity. Hence, the impact of the Gibbs phenomenon can be overcome.

A constructive approach to the identification of the complementary basis is currently unknown and subject to future research. The existence of such a basis, however, has been established by carefully examining the properties of the basis

$$\psi_n^\lambda(\xi) = C_n^{(\lambda)}(\xi) \ ,$$

where $C_n^\lambda(\xi)$ represent the Gegenbauer polynomials, also known as the symmetric Jacobi polynomials or the ultraspherical polynomials. We proved that this may serve as a complementary Gibbs basis to the Fourier basis, the Chebyshev polynomials and the Legendre polynomials.

We have focused on the resolution of the Gibbs phenomenon for continuous spectral expansions which, unfortunately, have little practical importance. A similar discussion and analysis for the discrete expansion is complicated by the introduction of the aliasing error. The proof that the Gegenbauer polynomials remain a Gibbs complementary basis for the Fourier and Chebyshev polynomials has be also completed

2.2 Convergence Results for Nonlinear Hyperbolic Problems

The return to the general nonlinear problem

$$\frac{\partial u}{\partial t} + \frac{\partial f(u)}{\partial x} = 0 \ , \tag{2.4}$$

introduces additional issues and new problems which are not relevant or of less importance for the variable coefficient problem.

One of the central difficulties in using spectral methods for the solution of nonlinear conservation laws lies in the potential development of nonsmooth solutions in finite time even for problems with very smooth initial conditions. As we have discussed previously, this introduces the Gibbs phenomenon which, through the nonlinearity, interacts with the solution. What we shall discuss in the following is the impact this has on the performance of the numerical approximation and techniques that allow us to recover accurate and physically meaningful solutions to the conservation laws even when the Gibbs oscillations are apparent.

2.2.1 Stability by the Use of Filters

Maintaining stability of the numerical approximation becomes increasingly hard as the discontinuity evolves and generates energy with higher and higher frequency content. This process, amplified by the nonlinear mixing of the Gibbs oscillations and the numerical solution, eventually renders the scheme unstable.

Understanding the source of the stability problem, i.e., accumulation of high frequency energy, also suggests a possible solution by introducing a dissipative mechanism that continuously remove these high frequency components.

A classical way to accomplish this is to modify the original problem by adding artificial dissipation as

$$\frac{\partial u}{\partial t} + \frac{\partial f(u)}{\partial x} = \varepsilon(-1)^{p+1}\frac{\partial^{2p} u}{\partial x^{2p}} \ .$$

A direct implementation of this, however, may be costly and could introduce additional stiffness which would limit the stable time step. We shall hence seek a different approach to reach a similar goal.

To understand the impact of using the filter at regular intervals as a stabilizing mechanism, consider the use of an exponential filter

$$\sigma(\eta) = \exp\left(-\alpha\eta^{2p}\right) \ .$$

As discussed in Sec. 2.1.1 this filter allows for a dramatic improvement in the accuracy of the approximation away from points of discontinuity.

To appreciate its impact on stability, consider the generic initial value problem

$$\frac{\partial u}{\partial t} = \mathcal{L}u \ ,$$

with the pseudospectral Fourier approximation

$$\frac{d}{dt}\boldsymbol{u} = \mathcal{L}_N\boldsymbol{u} \ .$$

Advancing the solution from $t = 0$ to $t = \Delta t$ followed by the filtering is conveniently expressed as

$$\boldsymbol{u}(\Delta t) = \mathcal{F}_N \exp(\mathcal{L}_N \Delta t)\boldsymbol{u}(0) \ .$$

If we first assume that $\mathcal{L}_N$ represents the constant coefficient hyperbolic problem, i.e., $\mathcal{L} = a\frac{\partial}{\partial x}$, we recover that

$$\tilde{u}_n(\Delta t) = \exp(-\alpha\eta^{2p} + a(ik)\Delta t)\tilde{u}_n(0) \ , \tag{2.5}$$

i.e., we are in fact computing the solution to the modified problem

$$\frac{\partial u}{\partial t} = a\frac{\partial u}{\partial x} - \alpha\frac{(-1)^p}{\Delta t N^{2p}}\frac{\partial^{2p} u}{\partial x^{2p}} \ .$$

The effect of the filter is thus equivalent to the classical approach of adding a small dissipative term to the original equation, but the process of adding the dissipation is very simple. Note in particular that $\Delta t N$ essentially represents the CFL condition and hence is of order one.

For a general $\mathcal{L}$, e.g., with a variable coefficient or of a nonlinear form, for which $\mathcal{F}_N$ and $\mathcal{L}_N$ no longer commute, the modified equation being solved takes the form

$$\frac{\partial u}{\partial t} = \mathcal{L}u - \alpha\frac{(-1)^p}{\Delta t N^{2p}}\frac{\partial^{2p} u}{\partial x^{2p}} + \mathcal{O}(\Delta t^2) \ ,$$

by viewing the application of the filter as an operator splitting problem [16]

With this in mind it is not surprising that using a filter has a stabilizing effect. Moreover, we observe that if p increases with N the modification caused by the filter vanishes spectrally as N increases. These loose arguments for the stabilizing effect of filtering have been put on firm ground for problem with smooth and nonsmooth initial data [77, 89] for the Fourier approximation to the general variable coefficient problem. These results, however, are typically derived under the assumption that $\sigma(\eta)$ is of polynomial form. While such filtering indeed stabilizes the approximation it may also reduce the global accuracy of the scheme [77, 42]. Let us therefore briefly consider the stabilizing effect of using the exponential filter in the pseudospectral Fourier approximation of hyperbolic equations, known to be only weakly unstable.

Consider the filtered approximation on the form

$$\frac{\partial u_N}{\partial t} + \mathcal{I}_N\left(a(x)\frac{\partial u_N}{\partial x}\right) = \varepsilon_N(-1)^{p+1}\frac{\partial^{2p} u_N}{\partial x^{2p}} \ , \tag{2.6}$$

where the superviscosity term on the right can be implemented through a filter and

$$\varepsilon_N = \frac{\alpha}{\Delta t N^{2p}} \ .$$

To establish stability, let us rewrite Eq.(2.6) as

$$\frac{\partial u_N}{\partial t} + \mathcal{N}_1 u_N + \mathcal{N}_2 u_N + \mathcal{N}_3 u_N = \varepsilon_N(-1)^{p+1}\frac{\partial^{2p} u_N}{\partial x^{2p}} \ ,$$

where

$$\mathcal{N}_1 u_N = \frac{1}{2}\frac{\partial}{\partial x}\mathcal{I}_N a(x) u_N + \frac{1}{2}\mathcal{I}_N\left(a(x)\frac{\partial u_N}{\partial x}\right) \ ,$$

is the skew-symmetric form of the operator,

$$\mathcal{N}_2 u_N = \frac{1}{2}\mathcal{I}_N\left(a(x)\frac{\partial u_N}{\partial x}\right) - \frac{1}{2}\mathcal{I}_N\frac{\partial a(x) u_N}{\partial x} \ ,$$

and

$$\mathcal{N}_3 u_N = \frac{1}{2}\mathcal{I}_N\frac{\partial a(x) u_N}{\partial x} - \frac{1}{2}\frac{\partial}{\partial x}\mathcal{I}_N a(x) u_N \ .$$

To establish stability, consider

$$\begin{aligned}\frac{1}{2}\frac{d}{dt}\|u_N\|_N^2 = -[u_N, \mathcal{N}_1 v_N]_N &- [u_N, \mathcal{N}_2 u_N]_N \\ &- [u_N, \mathcal{N}_3 u_N]_N + \left[u_N, \varepsilon_N(-1)^{p+1}\frac{\partial^{2p} u_N}{\partial x^{2p}}\right]_N \ .\end{aligned}$$

Clearly $[u_N, \mathcal{N}_1 u_N]_N = 0$ due to the skew-symmetry of $\mathcal{N}_1 u_N$ and by inspection we can bound

$$[u_N, \mathcal{N}_2 u_N]_N \le \tfrac{1}{2}\max_{x\in[0,2\pi]}|a_x(x)|\|u_N\|_N^2 \ .$$

It is indeed the term associated with $\mathcal{N}_3 u_N$ that is the source of the problems. To appreciate this, note that if $\mathcal{P}_N$ was used rather than $\mathcal{I}_N$ such that differentiation and truncation commute, the term would vanishes identically and the scheme would be stable. To bound this term, we can use that

$$[u_N, \mathcal{N}_3 u_N]_N \leq C \left(\|u_N\|_N^2 + \|\mathcal{N}_3 u_N\|_N^2 \right) \ .$$

Noting that $\|\mathcal{N}_3 u_N\|_{L^2[0,2\pi]}^2$ is nothing more than the commutation error and that $\|\cdot\|_N$ is L^2-equivalent, we can obtain

$$[u_N, \mathcal{N}_3 u_N]_N \leq C \left(\|u_N\|_{L^2[0,2\pi]}^2 + N^{2-2p} \|u_N^{(p)}\|_{L^2[0.2\pi]}^2 \right) \ ,$$

where C depends on $a(x)$ and its first p derivatives. If we finally note that

$$\left[u_N, \varepsilon_N (-1)^{p+1} \frac{\partial^{2p} u_N}{\partial x^{2p}} \right]_N = -\varepsilon_N \|u_N^{(p)}\|_N^2 \ ,$$

it is clear that we can always choose $\varepsilon_N = A N^{2-2p}$ and A sufficiently large to ensure stability. In other words, using an exponential filter is sufficient to stabilize the Fourier approximation.

There is one central difference in the effect of using the filter in the Fourier and the Chebyshev approximation. In the latter, the modified equation takes the form

$$\frac{\partial u}{\partial t} = \mathcal{L} u - \alpha \frac{(-1)^p}{\Delta t N^{2p}} \left[\sqrt{1-x^2} \frac{\partial}{\partial x} \right]^{2p} u + \mathcal{O}(\Delta t^2) \ . \tag{2.7}$$

Hence, while the filtering continues to introduce dissipation, it is spatially varying. In particular, it vanishes as one approaches the boundaries of the domain. In computations with moving discontinuities this may be a source of problems since the stabilization decreases as the discontinuity approaches the boundaries of the computational domain.

2.2.2 Spectrally Vanishing Viscosity and Entropy Solutions

The foundation of a convergence theory for spectral approximations to conservation laws has been laid in [91, 75] for the periodic case and subsequently extended in [76] to the Legendre approximation and recently to the Chebyshev-Legendre scheme in [73, 74].

To appreciate the basic elements of this convergence theory let us first restrict ourselves to the periodic case. For the discrete approximation to Eq.(2.4) we must add a dissipative term that is strong enough to stabilize the approximation, yet small enough not to ruin the spectral accuracy of the scheme. In [91, 75] the following spectral viscosity method was considered

$$\frac{\partial u_N}{\partial t} + \frac{\partial}{\partial x} \mathcal{P}_N (f(u_N)) = \varepsilon_N (-1)^{p+1} \frac{\partial^p}{\partial x^p} \left[Q_m(x,t) * \frac{\partial^p u_N}{\partial x^p} \right] \ , \tag{2.8}$$

where

$$\frac{\partial^p}{\partial x^p} \left[Q_m(x,t) * \frac{\partial^p u_N}{\partial x^p} \right] = \sum_{m < |n| \leq N} (ik)^{2p} \hat{Q}_n \hat{u}_n \exp(inx) \ .$$

To ensure that stability is maintained m should not be taken too big. On the other hand, taking m too small will impact the accuracy in

a negative way. An acceptable compromise seems to be

$$m \sim N^\theta \ , \ \theta < \frac{2p-1}{2p} \ .$$

Moreover, the smoothing factors, $\hat{Q}_n$, should only be activated for high modes as

$$\hat{Q}_n = 1 - \left(\frac{m}{|n|} \right)^{\frac{2p-1}{\theta}} \ ,$$

for $|n| > m$ and $\hat{Q}_n = 1$ otherwise. Finally, we shall assume that the amplitude of the viscosity is small as

$$\varepsilon_N \sim \frac{C}{N^{2p-1}} \ .$$

Under these assumptions, one can prove for $p = 1$ that the solution is bounded in $L^\infty[0, 2\pi]$ and obtain the estimate

$$\|u_N\|_{L^2[0.2\pi]} + \sqrt{\varepsilon_N} \left\| \frac{\partial u_N}{\partial x} \right\|_{L^2_{loc}} \leq C \ .$$

Convergence to the correct entropy solution then follows from compensated compactness arguments [91, 75].

To realize the close connection between the spectral viscosity method and the use of filters discussed in Sec. 2.2.1, consider the simple case where $f(u) = au$. In this case, the solution to Eq.(2.8) is given as

$$\hat{u}_n(t) = \exp\left(inat - \varepsilon_N n^2 \hat{Q}_n\right) \hat{u}_n(0) \ , \quad |n| > m \ ,$$

which is equivalent to the effect of the filtering discussed in Sec. 2.2.1. Note that the direct application of the vanishing viscosity term in Eq.(2.8) amounts to $2p$ spatial derivatives while filtering as discussed in Sec. 2.1.1 can be done at little or no additional cost.

For $p \neq 1$ a bound on the $L^\infty[0, 2\pi]$ is no longer known. However, experience suggests that it is better to filter from the first mode but to employ a slower decay of the expansion coefficients, corresponding to taking $p > 1$. This yields the superviscosity method in which one solves

$$\frac{\partial u_N}{\partial t} + \frac{\partial}{\partial x} \mathcal{P}_N f(u_N) = \varepsilon_N (-1)^{p+1} \frac{\partial^{2p} u_N}{\partial x^{2p}} \ ,$$

which we recognize from Eq.(2.6) as being equivalent to that obtained when using a high-order exponential filter.

The vanishing viscosity approximation to Eq.(2.4) using a Chebyshev collocation approach takes the form

$$\frac{\partial u_N}{\partial t} + \frac{\partial}{\partial x} \mathcal{I}_N f(u_N) = \varepsilon_N (-1)^{p+1} \left[\sqrt{1-x^2} \frac{\partial}{\partial x} \right]^{2p} u_N + \mathcal{B} u_N \ ,$$

where again

$$\varepsilon_N \sim \frac{C}{N^{2p-1}} \ ,$$

and p grows with N [76]. Here the boundary operator, $\mathcal{B}u_N$, may vanish or it may take values as

$$\tau^- \frac{(1-x)T'_N(x)}{2T'_N(-1)} \left(u_N(-1,t) - g^-\right) \ ,$$

$$\tau^+ \frac{(1+x)T'_N(x)}{2T'_N(1)} \left(u_N(1,t) - g^+\right) \ ,$$

which we recognize as the weakly imposed penalty terms. Note again that the vanishing viscosity term is equivalent to that obtained from the analysis of the effect of spectral space filtering, Eq.(2.7). Similar results can be obtained for the Legendre approximation and for the Chebyshev-Legendre method for which convergence has been proven [73, 74], using arguments similar to those in [91, 75],

using arguments similar to those in [91, 75], for $p = 1$ as well as for $p > 1$.

2.2.3 Conservation

It is natural to question whether the introduction of the artificial Gibbs oscillations has any impact on the basic physical properties described by the conservation law, e.g., mass conservation and the speed by which discontinuities propagate.

To come to an understanding of this, assume a spatially periodic problem and consider the pseudospectral Fourier scheme

$$\frac{d}{dt}\boldsymbol{u} + \mathrm{D}\boldsymbol{f} = 0 \ ,$$

where $\boldsymbol{u} = [u_N(0,t),..,u_N(x_{2N-1},t)]^T$ represent the grid vector and the interpolation of the flux is given as $\boldsymbol{f} = [\mathcal{I}_N f(u_N(0,t),t),..,\mathcal{I}_N f(u_N(x_{2N-1},t),t)]^T$.

The first thing to note is that

$$\int_0^{2\pi} u_N(x,t)\,dx = \int_0^{2\pi} u_N(x,0)\,dx \ ,$$

as an immediate consequence of the accuracy of the trapezoidal rule and the assumption of periodicity. Hence, the

approximation conserves the 'mass' of the interpolation of the initial conditions.

Let us introduce a smooth periodic test function, $\psi(x,t)$, with the corresponding grid vector, $\boldsymbol{\psi} = [\psi_N(x_0,t),..,\psi_N(x_{2N-1},$ The test function, $\psi(x,t)$, is assumed to vanish at large t. If we consider [35]

$$\boldsymbol{\psi}^T\left(\frac{d}{dt}\boldsymbol{u} + \mathrm{D}\boldsymbol{f}\right) = 0 \ ,$$

and utilize the accuracy of the trapezoidal rule we recover

$$\int_0^{2\pi}\left[\psi_N(x,t)\frac{\partial u_N(x,t)}{\partial t} - \frac{\partial \psi_N(x,t)}{\partial x}\mathcal{I}_N f(u_N(x,t),t)\right]\,dx = 0 \ ,$$

after integration by parts which is permitted if the solution, $u_N(x,t)$, is bounded. This implicitly assumes that the numerical approximation itself is stable which generally implies that a vanishing viscosity term is to be added, potentially through the use of a filter.

Integrating over time and by parts once more, we recover the result

$$\int_0^{\infty}\int_0^{2\pi}\left[u_N(x,t)\frac{\partial \psi_N(x,t)}{\partial t} + \frac{\partial \psi_N(x,t)}{\partial x}\mathcal{I}_N f(u_N(x,t),t)\right]\,dx\,dt + \int_0^{2\pi}\psi_N(x,0)u_N(x,0)\,dx = 0 \ .$$

Thus, for $N \to \infty$ the solution, $u_N(x,t)$, is a weak solution to the conservation law. This essentially implies that the limit solution satisfies the Rankine-Hugoniot conditions which again guarantees that shocks propagate at the right speed to within the order of the scheme. Results similar to these have been obtained for the Chebyshev approximation to the conservation law [35].

To appreciate that the addition of the vanishing viscosity has no impact on the conservation of the scheme, consider the Legendre superviscosity case [76] and let $\psi(x,t)$ be a test function in $C^3[-1,1]$ that vanishes at the endpoints. Taking $\psi_{N-1}(x,t) = \mathcal{I}_{N-1}\psi(x,t)$, then clearly $\psi_{N-1}(x,t) \to \psi(x,t)$, $(\psi_{N-1})_x(x,t) \to \psi_x(x,t)$, and $(\psi_{N-1})_t(x,t) \to \psi_t(x,t)$ uniformly in N

Since $\psi_{N-1}(x)$ is a polynomial that vanishes on the boundaries we have

$$\int_{-1}^{1}(1+x)P_N'(x)\psi_{N-1}(x,t)\,dx \ = \ 0, \qquad \int_{-1}^{1}(1-x)P_N'(x)\psi_{N-1}(x,t)\,dx \ = \ 0.$$

Moreover, integration by parts yields that

$$\lim_{N\to\infty}\frac{\epsilon_N(-1)^p}{N^{2p-1}}\int_{-1}^{1}\psi_{N-1}(x,t)\left[\frac{\partial}{\partial x}(1-x^2)\frac{\partial}{\partial x}\right]^{2p}u_N(x,t)\,dx \ = \ 0$$

Hence, the superviscosity term does not cause any problems and one can show that

$$-\int_0^T\int_{-1}^{1}\left(u_N(x,t)\frac{\partial \psi_{N-1}(x,t)}{\partial t} + \mathcal{I}_N f(u_N(x,t))\frac{\partial \psi_{N-1}(x,t)}{\partial x}\right)\,dx\,dt - \int_{-1}^{1}u_N(x,0)\psi_{N-1}(x,0)\,dx \ = \ 0 \ .$$

The main conclusion of this is that if $u_N(x,t)$ is a solution to the Legendre collocation approximation at the Gauss-Lobatto points and if $u_N(x,t)$ converges almost everywhere to a function $u(x,t)$, then $u(x,t)$ is a weak

solution to Eq.(2.4). The technical details of this proof can be found in [14] where also a similar result for the Chebyshev superviscosity approximation is given.

The theory of convergence of spectral methods equipped with spectral viscosity or superviscosity is limited to the scalar case as discussed in Sec. 2.2.2. For the system case a more limited result can be obtained, stating that if the solution converges to a bounded solution, it converges to the correct weak solution.

3 Recessed Cavity Flameholders

In [29, 30] we applied the spectral penalty method to simulate supersonic combustion problems in recessed cavities in order to establish the efficacy of recessed cavity flame-holders.

We considered two different cases; (1)*Non-reactive flows with two chemical species* and (2)*Reactive flows with four chemical species.* (3)*Injector-cavity flows with four chemical species.*

Recessed cavities provide a high temperature, low speed recirculating region that can support the production of radicals created during chemical reactions. This stable and efficient flame-holding performance by the cavity is achieved by generating a recirculation region inside the cavity where a hot pool of radicals forms resulting in reducing the induction time and thus obtaining the auto-ignition. Experiments have shown that such efficiency depends on the geometry of the cavity such as the degree of the slantness of the aft wall and the length to depth ratio of cavity L/D. Thus one can optimize the flame-holding performance by properly adjusting the geometrical parameters of the cavity flame-holder system for a given supersonic flight regime. There are two major issues of such cavity flame-holder system that need to be investigated: (1) *What is the optimal angle of the aft wall for a given L/D?* and (2)*How does the fuel injection interact with cavity flows?* An answer to these questions require both a comprehensive laboratory and numerical experiments.

In this work, we solved the full compressible Navier-Stokes equations with chemical reactions without any turbulence model, using a multi-domain spectral method.

Results of several numerical studies including in the study have shown that the stability of the recirculation inside cavity is enhanced for the lower angle of cavity compared to the rectangular cavity. The present study, however, gives more accurate and finer details of the fields than those done by lower order numerical experiments. We show that a stationary recirculation region is not formed inside the cavity contrary to what the lower order schemes predict. A quantitative analysis made in this study shows that the lower angled wall of the cavity reduces the pressure fluctuations significantly inside the cavity for the non-reactive flows. We obtained a similar result for the reactive flows with the ignition of the fuel supplied initially in the cavity.

The Injector-cavity system was also considered with the hydrogen fuel of $M = 1$, constantly injected ahead of cavity, and we investigated how cavity plays a role as a flame-holder and how the recessivity of cavity could affect the flame-holding efficiency of this system.

The results show that the pressure fluctuations in cavities with lower angle of the aft are weaker than in cavities with higher angles. It is also shown that the attenuation of the pressure fluctuations are obtained both at the center and the middle of the floor of the cavity. We also show that the large recirculation zone(s) formed inside the cavity obtained by the lower order numerical scheme is induced not physically but rather artificially due to the heavy numerical dissipations. This result shows that for these sensitive problems, high order accuracy should be used in order to minimize the effect of the numerical dissipation.

We also considered the case of the reactive flows for the 90 and 30 degree aft walls. Similar features of the pressure fluctuations are shown as in the non-reactive flows. However the pressure fluctuations are much more attenuated for both the 90 and 30 degree walls than in the non-reactive cold flows. These results demonstrate that simulations of cold flows do not necessarily shed light on the behavior of reactive flows. The shear layer is becoming weaker as the degree of angle of the aft wall is getting low and the flow fields are becoming more regularized for the case of the lower angled wall.

$t = 0.175ms$

$t = 0.275ms$

$t = 0.945ms$

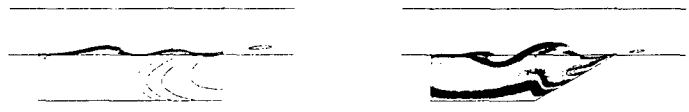

$t = 2.26ms$

Figure 1: The water contour of the reactive flows: the water density contours are given in the left figures for the 90° wall 30° wall in the right. From top to bottom the instant times t are $0.175ms$, $0.275ms$, $0.945ms$ and $2.26ms$ respectively. The maximum and minimum contour levels are 0.01 and 0.23 respectively with the number of levels 50.

Figure 1 shows the water contour inside the cavity for the different angles at different time. Here we define the region where the flames are generated to be same as the region where the water is produced. As the Hydrogen fuel is consumed, the water is produced and starts to be expelled from the cavity to the main channel. Figure 1 shows that the lower angled wall cavity (30° in this case) maintains more water than the 90° wall cavity at a given time. The figure also shows that the lower angled aft wall holds the flame (water in this case) longer than the 90° wall cavity.

These results imply that the flame-holding efficiency can be increased by lowering the angle of the aft wall of the cavity.

4 WENO methods

These are methods using either locally adaptive, nonlinear weighted stencils in performing high order interpolations or reconstructions, for problems containing both shocks and complicated smooth structures in their solutions. Weighted ENO schemes have been developed in the last years and applied successfully to simulate shock turbulence interactions to the direct simulation of turbulence ; to detonation shock dynamics , to dynamical response of a stellar atmosphere to pressure perturbations ; to overheating problem in multimaterial compressible flows ; to large-eddy simulations ; to relativistic hydrodynamics equations ; to shock vortex interactions and other gas dynamics problems .to incompressible flow problems to semi-conductor device simulation ; to underwater blast-wave focusing ; to the composite schemes and shallow water equations , to real gas computations ; to viscoelasticity with fading memory ; to subpixel interpolation in image processing etc.

In the following we will briefly review recent advances concerning WENO (weighted essentially non-oscillatory) methods. in [8], Balsara and Shu have investigated very high order finite difference WENO schemes. The class of methods includes seventh, ninth, eleventh and thirteenth order methods, stabilized by a suitable monotonicity preserving bounds. It is verified that these methods are indeed uniformly accurate of the claimed high order accuracy, and they give non-oscillatory shock transitions in the presence of discontinuities. These methods have good potential for situations where extremely high order of accuracy is important, such as direct numerical simulation of turbulence. Further investigation to analyze and improve these methods is proposed in this proposal.

Also on WENO methods, Hu and Shu [59] have constructed high order weighted essentially non-oscillatory (WENO) schemes on two dimensional unstructured meshes (triangles) in the finite volume formulation. Third and fourth order schemes are constructed. Numerical examples are shown to demonstrate the accuracies and robustness of the methods for shock calculations. Further investigation to analyze and improve these methods is proposed in this proposal.

In [78], Montarnal and Shu have used a recently developed energy relaxation theory by Coquel and Perthame and high order weighted essentially non-oscillatory (WENO) schemes to simulate the Euler equations of real gas. A relaxation process is performed for each time step to ensure that the original pressure law is satisfied. The necessary characteristic decomposition for the high order WENO schemes is performed on the characteristic fields based on the simple γ-law, hence dramatically reduces the computational cost. The algorithm only calls for the original pressure law once per grid point per time step, without the need to compute its derivatives or any Riemann solvers. Both one and two dimensional numerical examples are shown to illustrate the effectiveness of this approach.

In [82] and [83], Shu has given two lectures notes to describe the construction, analysis, and application of ENO (Essentially Non-Oscillatory) and WENO (Weighted Essentially Non-Oscillatory) schemes for hyperbolic conservation laws and related Hamilton-Jacobi equations.

In [97], Zhou, Li and Shu first review WENO finite volume and discontinuous Galerkin finite element methods, pointing out their similarities and differences in algorithm formulation, theoretical properties, implementation issues, applicability, and relative advantages. They then present some quantitative comparisons of the third order finite volume WENO methods and discontinuous Galerkin methods for a series of test problems to assess their relative merits in accuracy and CPU timing.

WENO (Weighted Essentially Non-Oscillatory) finite difference methods are methods using either locally adaptive, nonlinear weighted stencils in performing high order interpolations or reconstructions, for problems containing both shocks and complicated smooth structures in their solutions. The methods are based on ENO schemes started with the pioneering work of Harten, Engquist, Osher and Chakravarthy [51]. ENO schemes based on point values and TVD Runge-Kutta time discretizations, which are efficient for multi-dimensional calculations, were designed in [84, 85]. Weighted ENO schemes have been developed in [72] for the third order finite volume version in 1D, and in [64] for third and fifth order finite difference version in 1D and multi space dimensions, with a general framework for the design of the smoothness indicators and nonlinear weights. Later, second, third and fourth order finite volume WENO schemes for 2D general triangulations have been developed in [27] and [59]. Very high order finite difference WENO schemes (for orders between 7 and 13) have been developed in [8]. Compact central WENO schemes have been developed in [68]. ENO and WENO have been successfully used to simulate shock turbulence interactions [85, 86, 5]; to the direct simulation of turbulence [86, 95]; to detonation shock dynamics [6], to dynamical response of a stellar atmosphere to pressure perturbations [17]; to overheating problem in multimaterial compressible flows [25]; to large-eddy simulations [32]; to relativistic hydrodynamics equations [18]; to shock vortex interactions and other gas dynamics problems [23, 48, 49, 61]; to incompressible flow problems [21, 50, 96]; to semi-conductor device simulation [24, 62]

;to Hamilton-Jacobi equations [79, 63]; to magnetohydrodynamics [65]; to wave-vortex interaction in rotating shallow water [66]; to the solution of Vlasov-Poisson equations [67]; to underwater blast-wave focusing [69]; to the composite schemes and shallow water equations [70, 71], to real gas computations [78]; to viscoelasticity with fading memory [87]; to subpixel interpolation in image processing [88]; etc. For a short summary of the development and applications of ENO and WENO schemes, see [81]. For a survey of ENO and WENO methods, see the lecture notes of Shu [82, 83].

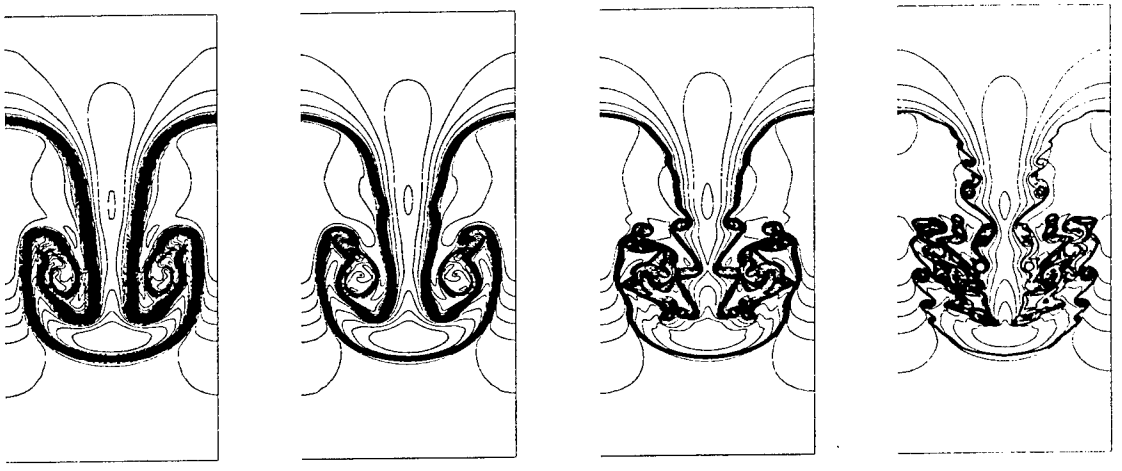

Figure 2: Rayleigh-Taylor, 5th WENO $\Delta x = \Delta y = \frac{1}{200}, \frac{1}{400}, \frac{1}{800}, \frac{1}{1600}$

Figure 3: Rayleigh-Taylor, 9th WENO $\Delta x = \Delta y = \frac{1}{200}, \frac{1}{400}, \frac{1}{800}, \frac{1}{1600}$

As an example, we can see from Fig. 2 and Fig. 3 that a ninth order WENO scheme computes the Rayleigh-Taylor instability problem much better than a fifth order WENO scheme, at about twice the CPU cost, on the same mesh. This indicates the advantage of going to high order accuracy for such problems. Such type of problems will be further investigated.

5 Multi-Domain Methods

The original motivation for the introduction of multi-domain methods can be found in the restrictions that the fixed grids, required to ensure the high spatial accuracy, impose. This fixed grid makes it difficult to utilize adaptivity and, for multi-dimensional problems, to address problems in complex geometries. Moreover, the use of global spectral expansions makes it difficult to achieve a high parallel efficiency on contemporary parallel computers.

Many of these concerns can be overcome if one splits the computational domain into a number of geometrically simple building blocks, e.g., squares and cubes, and then employs tensor-product forms of the simple one-dimensional approximations as the basis of an element by element approximation. While this technique opens up for the use of a highly non-uniform resolution and the ability to model problems in geometrically complex domains, it also introduces the need to connect the many local solutions in an accurate, stable, and efficient manner to reconstruct the global solution.

5.1 Patching Techniques

The patching of the local solutions in a way consistent with the nature of the hyperbolic problem can be performed in at least two different yet related ways. We shall refer to these two different methods as the differential and the correctional method, respectively.

To expose the differences between the two methods, let us consider the two domain scalar problem

$$\begin{aligned} \frac{\partial u}{\partial t} + \frac{\partial f(u)}{\partial x} &= 0 \ , \quad x \in [-1,0] \\ \frac{\partial v}{\partial t} + \frac{\partial f(v)}{\partial x} &= 0 \ , \quad x \in [0,1] \ . \end{aligned} \tag{5.1}$$

To recover the global solution $U = [u, v]$ under the constraint that $u(0,t) = v(0,t)$, the central issue is how one decides which of the multiple solutions at $x = 0$ takes preference and hence determines the evolution of $u(0,t)$ and $v(0,t)$.

Provided that the initial conditions are consistent with the continuity condition it will clearly remain continuous if we ensure that $u_t(0,t) = v_t(0,t)$. This approach, known as the differential method, involves the exchange of information between the two domains to ensure that the flux of $u(0,t)$ and $v(0,t)$ are identical throughout the computation. There are, however, several ways to do so.

In general one introduces the flux-derivative

$$\lambda = \left.\frac{\partial f}{\partial u}\right|_{u(0,t)} = \left.\frac{\partial f}{\partial v}\right|_{v(0,t)} \ ,$$

and requires that u and v be updated at $x = 0$ as

$$\left.\frac{\partial u}{\partial t}\right|_{x=0} = \left.\frac{\partial v}{\partial t}\right|_{x=0} = -\tfrac{1}{2}\left(\lambda + |\lambda|\right)\left.\frac{\partial u}{\partial x}\right|_{x=0} - \tfrac{1}{2}\left(\lambda - |\lambda|\right)\left.\frac{\partial v}{\partial x}\right|_{x=0} \ .$$

This can be recognized as nothing else than pure upwinding. The extension to systems of equations employs the characteristic form of the system and the multi-dimensional case is treated by dimensional splitting.

An alternative formulation, based on the weakly imposed boundary conditions introduced in [52, 58, 54], takes the form

$$\begin{aligned} \left.\frac{\partial u}{\partial t}\right|_{x=0} + \left.\frac{\partial f(u)}{\partial t}\right|_{x=0} &= -\tau\frac{|\lambda - |\lambda||}{2}\left(u(0,t) - v(0,t)\right) \ , \\ \left.\frac{\partial v}{\partial t}\right|_{x=0} + \left.\frac{\partial f(v)}{\partial t}\right|_{x=0} &= -\tau\frac{|\lambda + |\lambda||}{2}\left(v(0,t) - u(0,t)\right) \ , \end{aligned}$$

which again amounts to upwinding, although on a weak form. The advantage of this latter formulation is that it allows for establishing stability and it makes the enforcement of very complex interface conditions simple. The extension to systems employs the characteristic variables and is discussed in detail in [52, 54] while the multi-dimensional case is treated in [58]. Similar developments for methods employing multi-variate polynomials

[55, 56] or a purely modal basis defined on triangles and tetrahedra has recently been developed, pawing the way for the formulation of stable spectral methods for the solution of hyperbolic conservation laws using a fully unstructured grid.

Rather than correcting the local temporal derivative to ensure continuity of the flux across the interface one could choose to modify the solution itself. This observation provides the basic foundation for correctional methods in which both u and v is advanced everywhere within the each domain, leading to a multiplicity of solutions at $x = 0$. For the specific case discussed here, the correctional approach amounts to

$$u(0,t) = v(0,t) = \begin{cases} u(0,t) & \text{if } \lambda \geq 0 \\ v(0,t) & \text{if } \lambda < 0 \end{cases} ,$$

which we again recognize as upwinding. The system case is treated similarly by exploiting the characteristic variables. As for the differential methods, the use of the characteristics implicitly assumes a minimum degree of smoothness of the solution. However, as no information about the spatial derivatives are passed between domains, the correctional method imposes no constraints on the smoothness of the grid.

The main appeal of the correctional method is its simplicity and robustness and it has been utilized to formulate very general multi-domain method for problems in gas-dynamics, and in acoustics and elasticity, and electromagnetic.

Note that both methods employ the local flux-Jacobian, λ, which implicitly requires a certain amount of smoothness of the solution at the interface. A differential method overcoming this can be realized by borrowing a few ideas from classical finite volume methods.

Consider the cell averaged formulation

$$\frac{d\overline{u}_j}{dt} + \frac{f(u(x_{j+1/2})) - f(u(x_{j-1/2}))}{\Delta x_j} ,$$

where

$$\Delta x_j = x_{i+1/2} - x_{i-1/2} \ , \ \overline{u}_j = \frac{1}{\Delta x_j} \int_{x_{j-1/2}}^{x_{j+1/2}} u(s)\, ds \ .$$

Here $x_{j\pm 1/2}$ signifies the Chebyshev-Gauss-Lobatto grid and x_j refers to the interlaced Chebyshev-Gauss grid. No assumptions are made about the smoothness of the flux and since each individual cell requires reconstruction, the patching of the subdomains is achieved by flux-splitting techniques known from finite volume methods. This approach was first proposed for Fourier methods and subsequently for the Chebyshev approximation and has the advantage of being conservative by construction. The averaging and reconstruction procedure, which can be done in an essentially non-oscillatory way, is essential for the accuracy and stability of the scheme and several alternatives, exploiting a similar framework, has been also proposed.

The use of a staggered grid, collocating the solution u at the Gauss grid and the fluxes, $f(u)$, at the Gauss-Lobatto grid, has the additional advantage of allowing for the formulation of multi-dimensional multi-domain methods with no grid points on the vertices of the elements. This approach has been developed for smooth problems and eliminates complications associated with the treatment of vertices in multi-domain methods.

5.2 Conservation Properties of Multi-Domain Schemes

The important question of the conservation properties of multi-domain schemes is discussed in [14] in which the following polynomial approximation to Eq.(5.1) is considered

$$\begin{aligned} \frac{\partial u_N}{\partial t} + \frac{\partial}{\partial x}\mathcal{I}_N f(u_N) = \quad & \tau_1 Q_I^+(x) \left[f^+(u_N(0,t)) - f^+(v_N(0,t))\right] \\ & + \tau_2 Q_I^+(x) \left[f^-(u_N(0,t)) - f^-(v_N(0,t))\right] + SV(u_N) \\ \frac{\partial v_N}{\partial t} + \frac{\partial}{\partial x}\mathcal{I}_N f(v_N) = \quad & -\tau_3 Q_{II}^-(x) \left[f^+(v_N(0,t)) - f^+(u_N(0,t))\right] \\ & - \tau_4 Q_{II}^-(x) \left[f^-(v_N(0,t)) - f^-(u_N(0,t))\right] + SV(v_N) \ , \end{aligned}$$

where $Q^{\pm}(x)$ are polynomials that vanish at all collocation points except $x = \pm 1$. Furthermore, $SV(u_N)$ and $SV(v_N)$ represent the vanishing viscosity terms, or filtering, required to stabilize the nonlinear problem as

discussed in Sec. 2.2.1 and Sec. 2.2.2, while $f = f^+ + f^-$ signifies a splitting into the upwind and downwind components of the flux.

To establish conservation of the approximation, consider a test function $\psi(x)$ and denote by ψ_I and ψ_{II} its restriction to the first and second domain respectively. We can assume that ψ_I and ψ_{II} are polynomials of order $N-1$ and that ψ_I vanishes at $x=-1$ of the first domain while ψ^{II} vanishes $x=1$ of the second domain, but not at $x=0$.

Repeated integration by parts using the fact that ψ_I vanishes on the left boundary and that $SV(u_N)$ vanishes at the boundaries of each domain yields

$$\int_{-1}^{0} \psi_I(x) SV(u_N)\, dx = u_N SV(\psi_I)$$

which tends to zero with increasing N. A similar result can be obtained for the second domain.

Consider now

$$\int_{-1}^{0} \psi^I(\dot{x}) \frac{\partial u}{\partial t}\, dx + \int_{0}^{1} \psi^{II}(x) \frac{\partial v_N}{\partial t}\, dx \ .$$

To recover that u_N and v_N are weak solutions to Eq.(5.1), i.e., the above integral vanishes, we must require

$$\tau_1 + \tau_3 = 1 \ , \ \tau_2 + \tau_4 = 1 \ . \tag{5.2}$$

However, for linear stability one can show that

$$\tau_1 \geq \frac{1}{2} \ , \ \tau_2 \leq \frac{1}{2} \ ,$$
$$\tau_3 \leq \frac{1}{2} \ , \ \tau_4 \geq \frac{1}{2} \ ,$$

are necessary and sufficient to guarantee stability.

This leaves us with a set of conditions under which to design stable and conservative scheme. In particular, if we choose to do pure upwinding at the interfaces by specifying

$$\tau_1 = \tau_4 = 1 \ , \ \tau_2 = \tau_3 = 0 \ ,$$

we essentially recover the discontinuous Galerkin method.

$$\tau_1 = \tau_2 = \tau_3 = \tau_4 = \frac{1}{2} \ ,$$

which yields a marginally stable and conservative scheme on the form

$$\begin{aligned} \frac{\partial u_N}{\partial t} + \frac{\partial}{\partial x}\mathcal{I}_N f(u_N) &= \frac{1}{2} Q_I^+(x) \left[f(u_N(0,t)) - f(v_N(0,t)) \right] + SV(u_N) \\ \frac{\partial v_N}{\partial t} + \frac{\partial}{\partial x}\mathcal{I}_N f(v_N) &= -\frac{1}{2} Q_{II}^-(x) \left[f(v_N(0,t)) - f(u_N(0,t)) \right] + SV(v_N) \ , \end{aligned}$$

i.e., the interface boundary conditions are imposed on the fluxes f rather than on the split fluxes f^+ and f^-.

5.3 Computational Efficiency

An interesting question pertaining to the use of multi-domain methods is how one decides how many elements and what resolution to use within each element. In pragmatic terms, what we are interested in is to identify the optimal combination of the order of the polynomial, N, and the number of elements, K, needed to solve a particular problem to within a maximum error using minimum computational resources. On one hand, it is the high order of the interpolation polynomial that yields the very accurate approximation. On the other hand, the computation of derivatives generally scales as $\mathcal{O}(N^2)$ while the total work scales only linearly with the number of elements. To develop guidelines for choosing the optimal N and K, consider a one-dimensional wave problem with a smooth solution. Assume that the approximation error, $E(N,K)$, scales as

$$E(N,K) \propto \left(\frac{\pi k}{KN}\right)^N \quad ,$$

where k is the maximum wavenumber in the solution, i.e., it is proportional to the inverse of the minimum spatial length scale. We shall require the maximum absolute error, E, is bounded as $E \leq \exp(-\gamma)$, and estimate the computational work as

$$W(N,K) = c_1 KN^2 + c_2 KN \quad ,$$

where c_1 and c_2 are problem specific constants. Minimizing the work subject to the error constraint yields the optimal values

$$N_{\text{opt}} = \gamma \quad , \quad K_{\text{opt}} = \frac{\pi k}{N_{\text{opt}}} \exp\left(\frac{\gamma}{N_{\text{opt}}}\right) \quad .$$

One observes that high accuracy, i.e., γ large, should be achieved by using a large number of modes, N, and not, as one could expect, by employing many subdomains each with a low number of modes. For very smooth and regular functions, where k is small, or if only moderate accuracy is required a multi-domain approach may not be the optimal method of choice. On the other hand, if the function exhibits strongly localized phenomena, i.e., k is large, one should introduce several domains to minimize the computational burden. While these arguments are loose, they indicate that an optimal choice of N and K for most problems seems to be a few larger subdomains, each with a reasonable number of modes to maintain an acceptable spatial accuracy.

These results have been confirmed in computational experiments in [52, 58, 57] indicating that $N = 8 - 16$ is reasonable for two-dimensional problems and $N = 4 - 8$ is reasonable for three-dimensional problems. If this results in insufficient resolution one should generally increase the number of domains rather than the resolution. Similar conclusions have been reached for the analysis of spectral multi-domain methods in a parallel setting [26].

6 Richtmyer Meskhov Instability (RMI)

Inertial Confinement Fusion Program (ICF) uses high energy pulse sources such as X-rays and lasers to illuminate the target sphere in order to achieve auto fusion ignition and such is the plan for the future on the National Ignition Facility (NIF) at Lawrence Livermore National Laboratory (LLNL). It is crucial to achieve uniform compression of the target sphere in order to obtain maximum efficiency as the impulsively accelerated non-uniform sphere surface by a shock wave causes a non-uniform pressure profile over the sphere. One can observe a similar phenomenon in the mixing of fuel with oxidants in a SCRAMJET engine, the fuel jets are under impulsive acceleration by shockwave . The fuel mixing efficiency is enhanced by the stretching of the fuel-oxidant interface and the breakup of fuels into finer droplets. The source of these two phenomena are known as the Richtmyer-Meshkov Instability (RMI) and they are related to the well known fluid instability studied theoretically by Richtmyer and experimentally by Meshkov.

In a word, the RMI results from an impulsively accelerated interface of materials with different densities under perturbation. This form of instability is different from the closely related fluid instability known as the Rayleigh-Taylor instability in which the material interface is under a constant acceleration force such as gravity. The vorticity generated by the cross product of the pressure gradient and the density gradient deforms and amplifies the interface perturbation and grows in time. The penetration of the heavier fluid into the lighter fluid forms spikes and bubbles and vice versa. A turbulence mixing zone of the two fluids is created and grows with time.

In order to capture the shock-interface interaction and the fine scale structures within the turbulence mixing zone, high order methods are highly desirable. From the point of view of the numerical calculation, we can break the RMI problem into two parts. First, we have the issue of reliably calculating the motion of a possibly very strong shock wave, and second we have the issue of reliably calculating the mix that ensues after this shock wave accelerates the interface. It is in this second area of calculating the ensuing mix where high order numerical schemes offer unparalleled efficiency. This efficiency comes from the very fundamental fact that the truncation error in the differentiation operators can be made much smaller by increasing the order of the scheme than by increasing the number of grid points. One of the consequences of this ability to rapidly reduce the truncation error is that long-time integration is computationally much less expensive with high order schemes, than with low order schemes. Further, when the flow contains small scale features such as in turbulent flows, high order numerical operators are far more efficient than low order operators, see [98], and adapting a low order scheme can not overcome the efficiency of a high order scheme. Among the high orders schemes considered, Spectral methods (Spectral) and Weighted Essentially Non-Oscillatory finite difference schemes (WENO) are considered in this study. High Order compact schemes are another candidate but was not considered in this study. High order, in the sense, means an order of accuracy higher than two. The numerical schemes developed here will served as a basis for the validation of the results obtained from both experiments and other numerical methods.

The governing equations are the two/three-dimensional Euler equations in Cartesian coordinates describing the conservation of mass, momentum and energy. The physical domain is a rectangular domain with $0 \leq x \leq L_x$ and $0 \leq y \leq \lambda$, where L_x is the user specified domain length in x and λ is the wave length of a single mode perturbation along the interface separating two different gases in the y direction. In this study, the gases are Xenon (Xe) and Argon (Ar). The specific heat ratio γ is assumed to be the same for both gases, $\gamma = \frac{5}{3}$.

The initial conditions (see figure 4) is an incident shock of Mach number $M = 4.46$ located at $x_s = 0.05cm$ that travels downstream toward the interface. Given the shock Mach number M, temperature T in the pre-shock region, and the density of the Xenon gas ρ_{Xe}, the initial condition of the flow satisfies the Hugoniot-Rankine Condition for normal steady shock, i.e.,

$$T_2 = T \ , \rho_2 = \rho_{Xe} \ , P_2 = R\rho_2 T_2 \ , C_2 = \sqrt{\gamma P_2/\rho_2} \ , U_2 = MC_2 \ , V_2 = 0$$

$$P_1 = P_2 \frac{2\gamma M^2 - (\gamma - 1)}{\gamma + 1} \ , \rho_1 = \rho_2 \frac{(\gamma + 1)M^2}{(\gamma - 1)M^2 + 2} \ , T_1 = P_1/(R\rho_1) \ , C_1 = \sqrt{\gamma P_1/\rho_1} \ , U_1 = U_2\rho_2/\rho_1 \ , V_1 = 0$$

The subscripts 1 and 2 denote the pre-shock and post-shock condition, respectively. To specify condition for the moving shock, the shock speed $s = MC_2$ is subtracted from the pre- and post- shock velocity U_1 and U_2, respectively. Using the cgm units, the constant $R = R_0/M_{Xe}$, where $R_0 = 8.31441 \times 10^7 \ \frac{erg}{K}$ is the universal gas constant, $M_{Xe} = 131.29 \ \frac{g}{g-mole}$ and $M_{Ar} = 39.948 \ \frac{g}{g-mole}$ are the molecular weight of Xenon and Argon, respectively.

In the pre-shock region, the temperature $T = 296.0 \ K$ and the density of Argon and Xenon gases are $\rho_{Ar} = 0.89 \times 10^{-3} \ \frac{g}{cm^3}$ and $\rho_{Xe} = 2.9 \times 10^{-3} \ \frac{g}{cm^3}$ respectively. The pressure is assumed to be half of the normal

atmospheric pressure.

Once the pre- and post- shock states of Xenon gas are specified, the region of Argon gas will be superimposed onto the pre-shock region replacing the Xenon gas. The diffused interface between the two gases is further perturbed to form a sinusoidal wave with some finite thickness with amplitude $a = 1.0\ cm$ and wave length $\lambda = 3.6\ cm$.

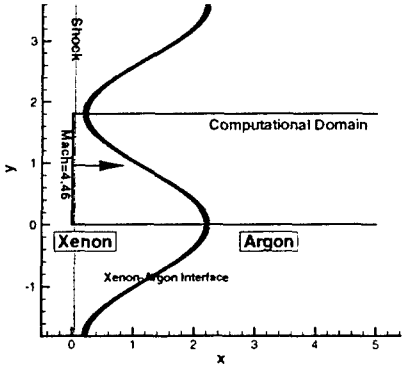

Figure 4: Initial Condition of the Richtmyer-Meshkov instability problem.

Solution Procedure :

1. Periodical Domain is specified in the y direction and symmetry property of the problem is exploited to reduce the amount of computational operations by half.
2. A combined Chebyshev and Fourier collocation methods is used to discretize the Euler equations in space yielding a Spectral scheme. A WENO-LF-5 fifth order finite difference scheme is also employed for the solution of the problem.
3. The high-performance parallel library PseudoPack, written by Bruno Costa and Wai Sun Don, is utilized for both Spectral scheme.
4. The third order TVD Runge Kutta method by Shu and Osher is used to advance the solution in time.
5. For the Spectral scheme, a 10'th and 9'th order exponential filter is used for the differentiation and solution smoothing respectively, at each Runge Kutta step unless otherwise specified.

As evidenced from the results of the Spectral and the WENO calculations shown below, the following major features of the Richtmyer-Meshkov instability can be observed (see figure 5) at time $t = 50 \times 10^{-6} s$, namely,

- Wave generated by the shock refraction behind the gas interface in Box 1.
- The penetration of the heavy (Xe) to light (Ar) fluid causes the deformation of the interface into a large mushroom shape structures in Box 2 and the opposite in Box 5. They are refered as Spike and Bubble respectively, in the literatures. They move in the opposite direction relative to each other and form a ever larger turbulence mixming zone.
- Pressure wave along the transmitted shock in Box 3.
- A small jet and its vortical structure located in Box 4. The contact discontinuity develops into a more complicated vortical rollups in a finer and long term simulation possibly caused by the Kelvin-Helmholtz instability.
- Vortical rollups of the gaseous interface inside Box 6.

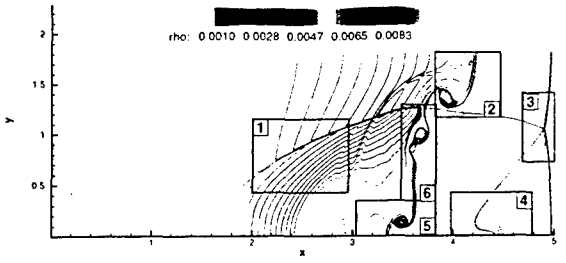

Figure 5: The numbered regions enclose the most prominent flow features of the Richmyter-Meshkov instability at time $t = 50 \times 10^{-6} s$.

The Mach number M, the Atwood number At and the interface curvature play an important role on the growth of perturbed amplitude on the interface. In the particular set of parameters studied here with high Mach number $M = 4.46$ and median Atwood number $At \approx 0.54$, a formation of triple-shock configuration along the interface indicates that shock-interface interaction is in the "hard" regime. A "hard" regime, as quoted from Zaytsev et al. [101] is "the propagation of secondary shocks across the flow that is accompanied by the formation of breaks and triple configurations on the refracted and reflected shocks". The triple-shock formation can be observed easily in the early time $<\approx 30 \times 10^{-6} s$.

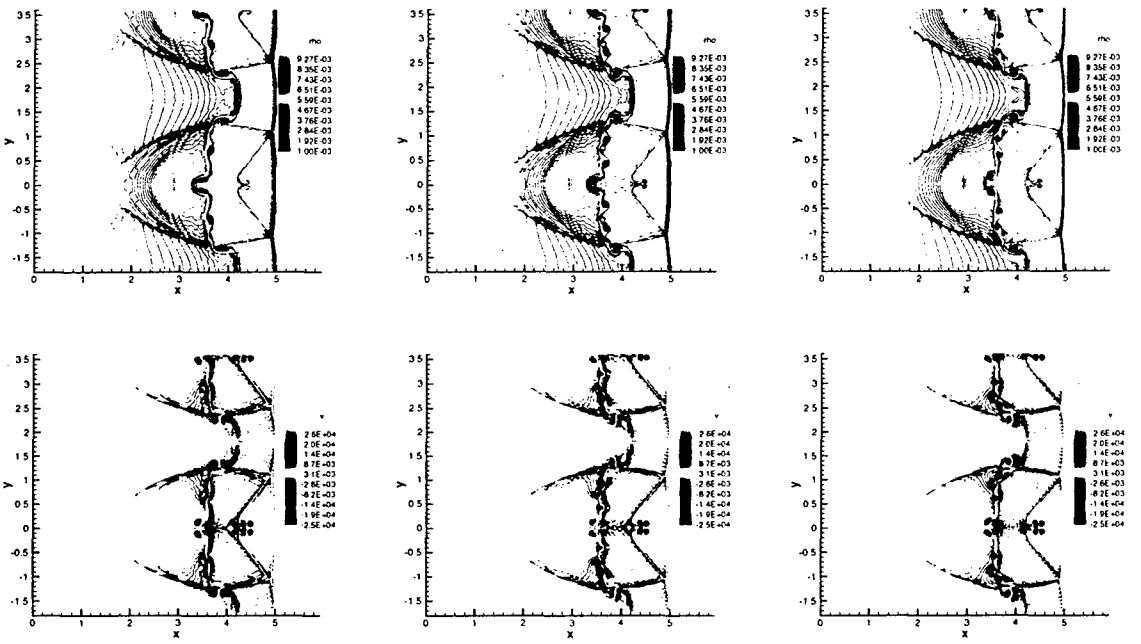

Figure 6: Density (Top Row) and V-Velocity (Bottom Row) contour plot of the Richtmyer-Meshkov instability as computed by the Spectral scheme. Domain length in x is $L_x = 5\ cm$. The interface thickness $\delta = 0.2\ cm$. The final time is $t = 50 \times 10^{-6} s$. The resolution of the Spectral schemes are 384x192 (Top Left), 512x256 (Top Right) and 1024x256 (Bottom Left).

The density ρ, velocity U and V and total energy E of the solution of the Spectral scheme figures (6) and and WENO-LF-5 scheme figures (7) and at time $t = 50 \times 10^{-6}\ s$ at various resolutions.

It can be observed that the large and median scale structures such as transmitted shock, shocked-interface velocity and shock triple point are basically in excellent agreement with each others. Some discrepancies of the fine scale structures along the gaseous interface, as can be expected for numerical simulation of the Euler equations which is sensitive to perturbation in nature, are observed.

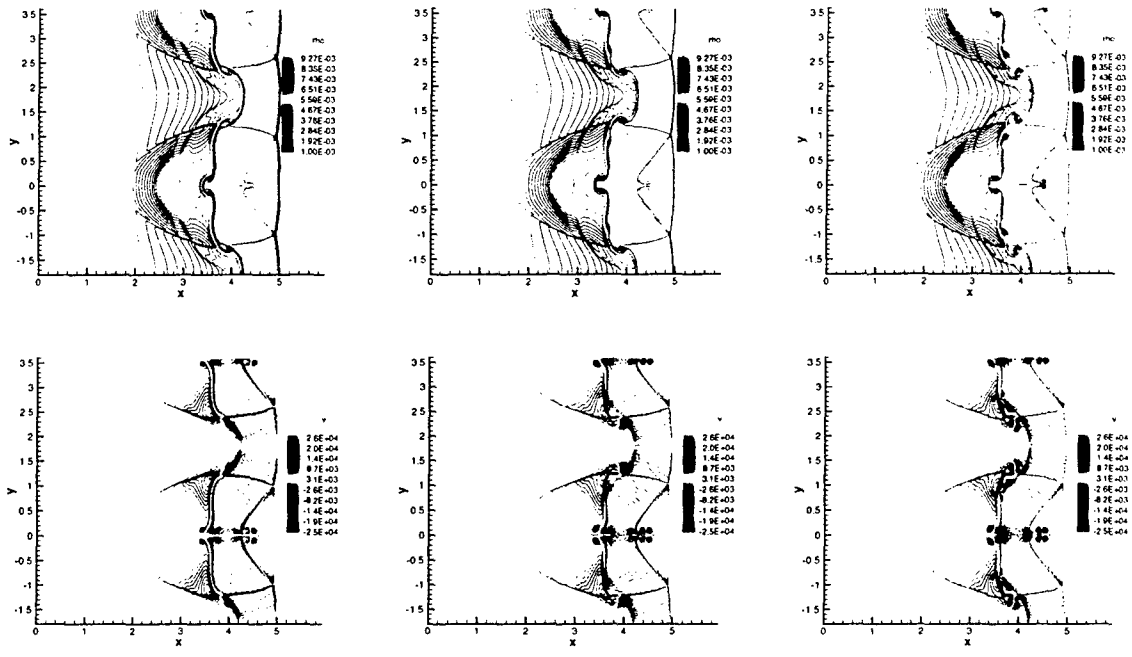

Figure 7: Density (Top Row) and V-Velocity (Bottom Row) contour plot of the Richtmyer-Meshkov instability as computed by the WENO-LF-5scheme. Domain length in x is $L_x = 5\ cm$. The final time is $t = 50 \times 10^{-6} s$. The resolution of the WENO-LF-5 schemes are 256x128 (Top Left), 512x256 (Top Right) and 1024x512 (Bottom Left).

The amplitude of the perturbed interface a is first decreased by the compression of the shock wave. The interface is then accelerated by the shock and grows from 2 cm to $\approx 2.6\ cm$ at time $143 \times 10^{-6} s$. Quantitatively, the amplitude growth rate a was plotted verus the mean displacement distance X_{K12} for various initial amplutides a_0 and Mach number M. It seems to match the experimental data given in figure 1.9 in the paper by Zaytsev et al. [101] for the case of initial amplitude $a_0 = 1\ cm$ and the distance passed by shock after interaction with the interface $X_{K_{12}} \approx 13\ cm$. It is consistent with the experimental observations for the linear growth of a within "soft regular" regime and decrease growth of a within the irregular regime.

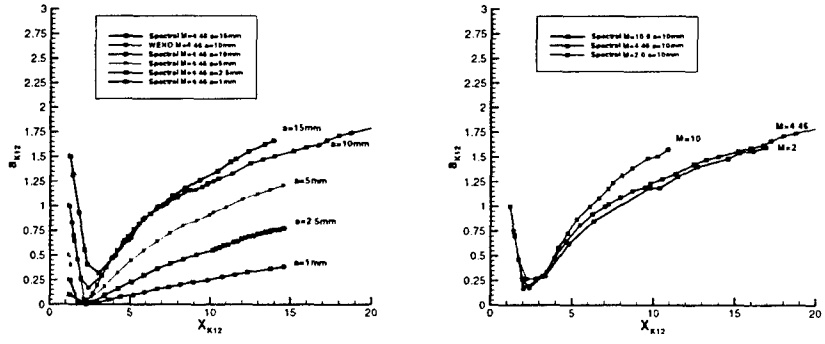

Figure 8: Growth rate of the amplitude (Left) and distance of interface traveled (Right).

7 Unstructured Spectral and WENO Schemes

While the structured grid multi-domain schemes described above are accurate, stable and robust, they suffer from two main disadvantages that makes the use of them difficult for certain classes of problems. It is well known that automated grid generation from CAD files is very complex when the geometric building blocks are curvilinear cubes only. Moreover, for problems with strongly local behavior, amenable to a space-time adaptive approach, a structured method is complicated by the need to propagate grid refinements through the grid or, alternatively, to use a non-conforming discretizations. To directly address these concerns, we have recently initiated a concentrated effort focused on the development of methods for solving the Navier Stokes equations in complex geometries using an unstructured grid.

We built upon an existing unstructured grid high-order framework, USEMe (Unstructured Spectral Element Method), in which the computational problem is assumed described by a collection of nonoverlapping simplices. It is furthermore assumed, as in finite element methods, that the simplex-based discretization is fully body-conforming but, contrary to classical finite element methods, we allow the simplices to include higher order information of the boundaries and interfaces, i.e., the simplices are fully bodyconforming with the possibility of curved edges and faces. This enables the use of large higher order elements while maintaining a geometry description to the order of the scheme.

Within each of the simplices the solution is assumed to be polynomial as

$$\boldsymbol{q}(\boldsymbol{x},t) \simeq \boldsymbol{q}_N(\boldsymbol{x},t) = \sum_{i=1}^{N} \boldsymbol{q}(\boldsymbol{x}_i,t) L_i(\boldsymbol{x}) \ ,$$

where $L_i(\boldsymbol{x})$ represents the truly multidimensional n'th order Lagrange interpolation polynomial based on the $N = \frac{1}{6}(n+1)(n+2)(n+3)$ nodal points, $\boldsymbol{x}_i$, within the tetrahedron.

The fully unstructured grid approach with high-order representations of the solutions directly addresses the need to provide a scheme with high order accuracy. Very significant geometric flexibility is furthermore ensured by the possibility of utilizing exiting geometry description and automated grid generation tools from finite-element methods.

It is worth while emphasizing that the boundary/interface conditions are not imposed exactly but rather weakly through the penalizing surface integral and that the formulation is inherently discontinuous, enforcing the interface conditions weakly through the penalizing term and giving rise to a highly parallel formulation of the scheme.

7.1 Weighted Essentially Nonoscillatory(WENO) Methods

The other extreme is to choose a local zeroth order basis in which case $\boldsymbol{q}_N$ now takes the role of the cell average and the high-order scheme described in the above reduces to a classical unstructured grid finite-volume scheme. In this scenario high-order accuracy is achieved in the reconstruction phase of the fluxes at the element interfaces although the particular choice of fluxes at the element phases also severely impact the performance of the scheme.

The central idea in the weighted essentially non-oscillatory(WENO) methods is to use locally adaptive, nonlinear weighted stencils to perform the high order reconstructions, borrowing ideas from ENO schemes. Both ENO and WENO methods have proven themselves very successful in solving problems dominated by strong shocks but with significant small scale dynamics, e.g., mixing problems.

8 Wellposed Perfectly Matched Layers for Advective Acoustics

The ability to simulate accurately wave phenomena is important in several physical fields, e.g., electromagnetics, ambient acoustics, advective acoustics associated with a mean flow, elasticity and seismology.

Often the numerical simulations of such problems, due to limited computing resources, must be confined to truncated domains much smaller than the physical space over which the wave phenomena take s place. In such cases, numerical reflections of outgoing waves from the boundaries of the numerical domain can falsify the computational results. This artifact limits the overall order of accuracy of the algorithm used in the computation. This is particularly troublesome in cases where higher order of accuracy is required by mode resolution, storage availability, etc.

To deal with these type of problems local non-reflecting boundary conditions were derived for the wave equation by Engquist and Majda [22] and later by Bayliss and Turkel [9]. In practice, however, their effectiveness was limited. The notion of perfectly matched absorbing layers (PML) was introduced in the context of computational electro-magnetics by Berenger [11]. The idea behind PML is to attribute to the layers "material" properties that modify the original field equations so that the waves will decay in all directions of propagation in the layers. However, it has been shown by Abarbanel and Gottlieb [1] that the splitting technique used by Berenger, results in a set of P.D.E's which are only weakly well posed, i.e., they may become ill posed under certain perturbations - an example of which is provided in [1]. We have suggested in [3] a new approach, to derive the PML equations from purely mathematical considerations. This approach yields, in the CEM case, a stable family of PML equations.

It is straightforward to show that there is a one to one correspondence between the case of two-dimensional ambient acoustics (no mean flow) and transverse electromagnetic wave propagation. Hence the PML procedures of CEM may be applied to the case of ambient acoustics.

In [2] we considered the case of advected acoustics (non-vanishing mean flow) with the PML layers being normal and parallel to the mean flow,. we used an extension of the procedure used in [3] to construct the PML equations for the case of electromagnetics by means of a mathematical procedure.

We considered the propagation of waves induced in a uniform two dimensional subsonic flow, $(u_0, 0)$, of a compressible fluid, by small perturbations. This phenomenon is described by the linearized Euler equations for the perturbations of the density, ρ', and velocities, u' and v' as

$$\frac{\partial \rho'}{\partial \bar{t}} + \bar{u}_0 \frac{\partial \rho'}{\partial \bar{x}} + \bar{\rho}_0 \frac{\partial u'}{\partial \bar{x}} + \rho_0 \frac{\partial v'}{\partial \bar{y}} = 0 \ , \tag{6.1}$$

$$\frac{\partial u'}{\partial \bar{t}} + \bar{u}_0 \frac{\partial u'}{\partial \bar{x}} + \frac{\bar{c}_0^2}{\bar{\rho}_0} \frac{\partial \rho'}{\partial \bar{x}} = 0 \ , \tag{6.2}$$

$$\frac{\partial v'}{\partial \bar{t}} + \bar{u}_0 \frac{\partial v'}{\partial \bar{x}} + \frac{\bar{c}_0^2}{\bar{\rho}_0} \frac{\partial \rho'}{\partial \bar{y}} = 0 \ , \tag{6.3}$$

where we assumed isentropy of the flow, i.e $\bar{p}_0 = \bar{p}_0(\rho_0^-)$. The speed of sound $\bar{c}_0$ is given by $\bar{c}_0^2 = d\bar{p}_0/d\bar{\rho}_0$ where $\overline{p_0}, \overline{\rho_0}$ are the unperturbed pressure and density of the flow. The dimensional time and distances are given by $\bar{t}, \bar{x}$ and $\bar{y}$.

We non-dimensionalized this set of equations by using a reference length $\bar{x}_2 = \bar{y}_2 = L$ (usually the relevant size of the computational domain and the wavelength of the illuminating wave), and a reference time $\bar{t}_r = L/\bar{c}_0$. Similarly $\bar{\rho}_r = \bar{\rho}_0$ and $\bar{u}_r = \bar{v}_r = c_0$. With $M = \bar{u}_0/\bar{c}_0$, the resulting set of dimensionless equation is:

$$p_t + M\rho_x + u_x + v_y = 0 \ , \tag{6.4}$$

$$u_t + Mu_x + \rho_x = 0 \ , \tag{6.5}$$

$$v_t + Mv_x + \rho_y = 0 \ , \tag{6.6}$$

where the prime $((\cdot)')$ has been dropped from the perturbation quantities. The case of ambient acoustics is obtained by letting the Mach number $M \to 0$. This case has been discussed by Hesthaven [53], and is known to correspond exactly to the case of 2-dimensional electromagnetic. Hence, for $M = 0$, the solution of any smooth initial boundary value problem can be shown to be a superposition of plane waves on the form

$$\begin{pmatrix} \rho \\ u \\ v \end{pmatrix} \sim \begin{pmatrix} 1 \\ \alpha \\ \beta \end{pmatrix} e^{i\omega(t-\alpha x-\beta y)} \ , \tag{6.7}$$

resulting in a dispersion relation on the form

$$\alpha^2 + \beta^2 = 1 \ . \tag{6.8}$$

When $M \neq 0$, however, the resulting dispersion relation is much more complicated, and the analysis from the case of electromagnetics cannot easily be carried over to the case acoustics waves.

To overcome this difficulty equations (6.4)-(6.6) were transformed to a new set of coordinates,

$$\xi = x \ , \tag{6.9}$$

$$\eta = \sqrt{1 - M^2} y = \gamma y \ , \tag{6.10}$$

$$\tau = Mx + \gamma^2 t \ . \tag{6.11}$$

This transformation is related to the one utilized in [9] although with stretching applying in y rather than in x as in [9]. As we shall see shortly, this difference is crucial.

The transformed equations take the form (with $\gamma = \sqrt{1 - M^2}$),

$$v_\tau + M v_\xi + \gamma \rho_\eta = 0 \ , \tag{6.12}$$

$$u_\tau + \rho_\xi - \frac{M}{\gamma} v_\eta = 0 \ , \tag{6.13}$$

$$\rho_\tau + u_\xi + \frac{1}{\gamma} v_\eta = 0 \ . \tag{6.14}$$

Note that the order of the equations has been reorganized such that that for $M = 0, (\gamma = 1)$, one recovers the two-dimensional transverse electric set of Maxwells equations [92] through the simple transformation, $\rho \leftrightarrow H, u \leftrightarrow E_y, v \leftrightarrow -E_x$.. This is done purely for convenience.

The plane wave solutions in the stretched space (ξ, η, τ) are of the form

$$\begin{pmatrix} v \\ u \\ \rho \end{pmatrix} = \begin{pmatrix} q_1 \\ q_2 \\ q_3 \end{pmatrix} e^{i\omega(\tau - B\eta - \lambda\xi)} \tag{6.15}$$

For this ansatz to be a solution, λ must be the solvability eigenvalue of (6.12)-(6.14) after the substitution of (6.15). The three distinct eigenvalues are given as

$$\lambda_0 = 1/M \ , \tag{6.16}$$

$$\lambda_1 = \sqrt{1 - B^2} \triangleq A \ , \tag{6.17}$$

$$\lambda_2 = -\sqrt{1 - B^2} = -A \ . \tag{6.18}$$

with the three corresponding eigenvectors being

$$\vec{q}_0 = \begin{pmatrix} M \\ -\frac{M^2 B}{\gamma} \\ 0 \end{pmatrix} \ , \quad \vec{q}_1 = \begin{pmatrix} B\gamma \\ A - M \\ 1 - MA \end{pmatrix} \ , \quad \vec{q}_2 = \begin{pmatrix} B\gamma \\ -A - M \\ 1 + MA \end{pmatrix} \ . \tag{6.19}(a,b,c)$$

The λ_0-solution corresponds to the rightward moving vorticity wave whose amplitude tends to zero as $M \to 0$, see eq. (6.19a). The λ_1 and λ_2 solutions represent the two counter-propagating acoustic waves moving to the right and left, respectively, in the (ξ, η)-plane. Note that because of the specific transformation $x, y, t \to \xi, \eta, \tau$ the eigenvalues $\lambda_1 = A = -\lambda_2$ satisfy the standard dispersion relation

$$A^2 + B^2 = 1 \ , \tag{6.20}$$

analogous to (6.8). Note also that in the physical plane the expression $A^2 + B^2 = 1$ does not constitute a dispersion relation.

The set of equations (6.12)-(6.14) is to be solved on a finite computational domain contrary to the original analytical problem which is set on an infinite domain. We would like to ensure that waves leaving the domain are

not reflected back into it as that could otherwise interact with the solution and hence falsify it. The approach taken here is to surround the computational domain with finite width strips which must be defined such that the waves propagate into these absorbing layers without reflection, and decay as they continue their travels inside these layers. Moreover, we shall require that these properties are independent of the frequency as well as the angle of incidence of the incoming wave.

We suggested the following Layers:

The PML equations in the absorbing "inflow" ξ-layer are

$$v_\tau + Mv_\xi + \gamma\rho_\eta = -\sigma_x v + 2\sigma_x Q_x + \sigma_x^2 R_x + M\sigma_x' P_x \ , \tag{6.21}$$

$$u_\tau + \rho_\xi - \frac{M}{\gamma} v_\eta = -\sigma_x u \ , \tag{6.22}$$

$$\rho_\tau + u_\xi + \frac{1}{\gamma} v_\eta = -\sigma_x \rho \ , \tag{6.23}$$

$$\frac{\partial Q_x}{\partial \tau} = -\gamma\rho_\eta \ , \tag{6.24}$$

$$\frac{\partial P_x}{\partial \tau} = v - \sigma_x P_x \ , \tag{6.25}$$

$$\frac{\partial R_x}{\partial \tau} = Q_x \ . \tag{6.26}$$

Note that from a computational point of view (6.22)-(6.25) hardly add to the amount of computing. The quantity $\partial\rho/\partial\eta$ is evaluated in (6.22) and thus (6.24)-(6.26) weigh as three additional o.d.e's rather than 3 additional p.d.e's. Transforming the system (6.22)-(6.25) back to the physical space (x, y, t) yields

$$\frac{\partial v}{\partial t} + M\frac{\partial v}{\partial x} + \frac{\partial \rho}{\partial y} = -\sigma_x v + 2\sigma_x Q_x + \sigma_x^2 R_x + M\sigma_x' P_x \ ,$$

$$\frac{\partial u}{\partial t} + M\frac{\partial u}{\partial x} + \frac{\partial \rho}{\partial x} = -\sigma_x u - \sigma_x M\rho \ ,$$

$$\frac{\partial \rho}{\partial t} + M\frac{\partial \rho}{\partial x} + \frac{\partial u}{\partial x} + \frac{\partial v}{\partial y} = -\sigma_x \rho - \sigma_x M u \ ,$$

$$\frac{\partial Q_x}{\partial t} = -\gamma^2 \frac{\partial \rho}{\partial y} \ ,$$

$$\frac{\partial P_x}{\partial t} = \gamma^2 (v - \sigma P_x) \ ,$$

$$\frac{\partial R_x}{\partial t} = \gamma^2 Q_x \ .$$

Let us briefly consider the issue of wellposedness of this new set of equations. Clearly, since the equations for P_x and R_x are o.d.e.'s these have no effect on the issue of wellposedness. The equation for Q_x, however, may affect the wellposedness of the original set of equations. but we showed that it did not.

The PML equations for both the upper and lower η-layers of the form

$$v_\tau + Mv_\xi + \gamma\rho_\eta = 2\sigma_y Q_y + \sigma_y^2 R_y + \gamma\sigma_y' P_y \ ,$$

$$u_\tau + p_\xi - \frac{M}{\gamma} v_\eta = 0 \ ,$$

$$\rho_\tau + u_\xi + \frac{1}{\gamma} v_\eta = 0 \ ,$$

$$\frac{\partial Q_y}{\partial \tau} = \gamma\frac{\partial \rho}{\partial \eta} - 2\sigma Q_y - \sigma^2 R_y - \sigma_y' P_y \ ,$$

$$\frac{\partial P_y}{\partial \tau} = (\rho - \sigma P_y) \ ,$$

$$\frac{\partial R_y}{\partial \tau} = Q_y \ .$$

In the (x, y, t)-space the system is

$$\frac{\partial v}{\partial t} + M\frac{\partial v}{\partial x} + \frac{\partial \rho}{\partial y} = 2\sigma_y Q_y + \sigma_y^2 R_y + \sigma_y' P_y \ , \tag{6.27}$$

$$\frac{\partial u}{\partial t} + M\frac{\partial u}{\partial x} + \frac{\partial \rho}{\partial x} = 0 \ ,$$

$$\frac{\partial \rho}{\partial t} + M\frac{\partial \rho}{\partial x} + \frac{\partial u}{\partial x} + \frac{\partial v}{\partial y} = 0 \ ,$$

$$\frac{\partial Q_y}{\partial t} = \gamma^2 \left[\frac{\partial \rho}{\partial y} - 2\sigma_y Q_y - \sigma_y^2 R_y - \sigma_y' P_y\right] \ ,$$

$$\frac{\partial P_y}{\partial t} = \gamma^2[\rho - \sigma_y P_y] \ ,$$

$$\frac{\partial R_y}{\partial t} = \gamma^2 Q_y \ .$$

Wellposedness of this system follows directly for the observation that only spatial derivatives of the density is introduced which, as we saw for the system (6.27) for the ξ-layer, does not affect wellposedness.

The development of efficient and accurate absorbing boundary conditions for problems in acoustics and beyond remains a very significant challenge. What we have presented, however, provided a mathematical framework in which such development may be successful. Indeed, the development of a PML for the three-dimensional equations of acoustics is straightforward provided only that the mean flow can be considered spatially constant.

Of equal importance is the development of PML methods for problems involving smoothly varying mean flows, as in boundary layers and jets. While the mathematical tools developed so far certainly are applicable for sufficiently smooth variations, new developments are most likely needed to address the general variable coefficient problem.

References

[1] S. Abarbanel and D. Gottlieb, *A Mathematical Analysis of the PML Method*, J. Comput. Phys. **134**(1997), pp. 357-363.

[2] S. Abarbanel, D. Gottlieb and J.S. Hesthaven, *Well-posed Perfectly Mathched Layers for Advective Acoustics*, J. Compt. Phys.**154**(1999), pp.266-283.

[3] S. Abarbanel and D. Gottlieb, *On the Construction and Analysis of Absorbing Layers in CEM*, Appl. Numer. Math. **27**(1998), pp. 331-340.

[4] R. Abgrall, *Numerical discretization of first order Hamilton-Jacobi equations on triangular meshes*, Comm. Pure Appl. Math., (1994), pp.1339-1373.

[5] N. Adams and K. Shariff, *A high-resolution hybrid compact-ENO scheme for shock-turbulence interaction problems*, J. Comput. Phys., v127 (1996), pp.27–51.

[6] T. Aslam and D. Stewart, *Detonation shock dynamics and comparisons with direct numerical simulation*, Combust. Theor. Model, v3 (1999), pp.77-101.

[7] S. Augoula and R. Abgrall, *High order numerical discretization for Hamilton-Jacobi equations on triangular meshes*, J. Sci. Comput., to appear.

[8] D. Balsara and C.-W. Shu, *Monotonicity preserving weighted essentially non-oscillatory schemes with increasingly high order of accuracy*, J. Comput. Phys., v160 (2000), pp.405-452.

[9] A. Bayliss and E. Turkel, *Radiation Boundary Conditions for Wave-Like Equations*, Comm. Pure Appl. Math. **33**(1980), pp. 707-725.

[10] N. S. BANERJEE AND J. GEER, *Exponential Approximations Using Fourier Series Partial Sums.* ICASE Report No. 97-56, NASA Langley Research Center, VA. 1997.

[11] J.-P. Berenger, *A Perfectly Matched Layer for the Absorption of Electromagnetic Waves*, J. Comput. Phys. **114**(1994), pp. 185-200.

[12] W. CAI, D. GOTTLIEB AND C.W. SHU, *Essentially Nonoscillatory Spectral Fourier Methods for Shock Wave Calculations*, Math. Comp. **52**(1989), pp. 389-410.

[13] W. CAI, D. GOTTLIEB, AND A. HARTEN, *Cell Averaging Chebyshev Methods for Hyperbolic Problems.* In Computers and Mathematics with Applications. Academic Press, New York, 1990.

[14] M. H. CARPENTER, D. GOTTLIEB, AND C. W, SHU, *On the Law-Wendroff Theorem for Spectral Methods* – accepted to Journal of Scientific Computing.

[15] W. S. DON, *Numerical Study of Pseudospectral Methods in Shock Wave Applications*, J. Comput. Phys. **110**(1994), pp. 103-111.

[16] W. S. DON AND D. GOTTLIEB, *Spectral Simulation of Supersonic Reactive Flows*, SIAM J. Numer. Anal. **35**(1998), pp. 2370-2384.

[17] L. Del Zanna, M. Velli and P. Londrillo, *Dynamical response of a stellar atmosphere to pressure perturbations: numerical simulations*, Astron Astrophys., v330 (1998), pp.L13-L16.

[18] A. Dolezal and S. Wong, *Relativistic hydrodynamics and essentially non-oscillatory shock capturing schemes*, J. Comput. Phys., v120 (1995), pp.266–277.

[19] K. S. ECKHOFF, *On Discontinuous Solutions of Hyperbolic Equations*, Comput. Methods Appl. Mech. Engrg. **116**(1994), pp. 103-112.

[20] K. S. ECKHOFF, *Accurate Reconstructions of Functions of Finite Regularity from Truncated Series Expansions*, Math. Comp. **64**(1995). pp. 671-690.

[21] W. E and C.-W. Shu, *A numerical resolution study of high order essentially non-oscillatory schemes applied to incompressible flow*, J. Comput. Phys., v110 (1994), pp.39–46.

[22] B. Engquist and A. Majda, *Absorbing Boundary Conditions for the Numerical Simulation of Waves*, Math. Comp. **31**(1977), pp. 629-651.

[23] G. Erlebacher, M.Y. Hussaini and C.-W. Shu, *Interaction of a shock with a longitudinal vortex*, J. Fluid Mech., v337 (1997), pp.129-153.

[24] E. Fatemi, J. Jerome and S. Osher, *Solution of the hydrodynamic device model using high order non-oscillatory shock capturing algorithms*, IEEE Trans. Computer Aided Design of Integrated Circuits and Systems, v10 (1991), pp.232–244.

[25] R. Fedkiw, A. Marquina, B. Merriman, *An isobaric fix for the overheating problem in multimaterial compressible flows*, J. Comput. Phys., v148 (1999), pp.545-578.

[26] P. FISCHER AND D. GOTTLIEB, *On the Optimal Number of Subdomains for Hyperbolic Problems on Parallel Computers*, Int. J. Supercomput. Appl. High Perform. Comput. **11**(1997), pp. 65-76.

[27] O. Friedrich, *Weighted essentially non-oscillatory schemes for the interpolation of mean values on unstructured grids*, J. Comput. Phys., v142 (1998), pp.304-330.

[28] A. GELB AND D. GOTTLIEB, *The Resolution of the Gibbs Phenomenon for Spliced Functions in One and Two Dimensions*, Computers Math. Applic. **33**(1997), pp. 35-58.

[29] A Multidomain Method for Supersonic Reactive Flows, (with W.S Don and J.H. Jung) submitted to JCP

[30] Multi-domain spectral method approach to supersonic combustion of recessed cavity flame-holders, (with W.S. Don and J.H. Jung), to appear in the proceeding of JANNAF-2002.

[31] A. GELB AND E. TADMOR, *Enhanced Spectral Viscosity Approximations for Conservation Laws*, Appl. Numer. Math. 2000 – to appear.

[32] E. Garnier, M. Mossi, P. Sagaut, P. Comte and M. Deville, *On the use of shock-capturing schemes for large-eddy simulation* J. Comput. Phys., v153 (1999), pp.273-311.

[33] D. Gottlieb and J. Hesthaven *Spectral Methods for Hyperbolic P roblems*, J. Comput. Appl. Math. vol. 128(1-2)(2001), pp. 83-131.

[34] B. Gustafsson and D. Gottlieb *On the direct Fourier method for computer tom ography*, IEEE Transactions on Medical Imaging, Vol.19, No. 3 pp.223-232 (2000).

[35] D. GOTTLIEB, L. LUSTMAN, AND S. A. ORSZAG, *Spectral Calculations of One-Dimensional Inviscid Compressible Flows*, SIAM J. Sci. Comp. **2**(1981), pp. 296-310.

[36] D. GOTTLIEB, L. LUSTMAN, AND E. TADMOR, *Stability Analysis of Spectral Methods for Hyperbolic Initial-Boundary Value Systems*, SIAM J. Numer. Anal. **24**(1987), pp. 241-256.

[37] D. GOTTLIEB, L. LUSTMAN, AND E. TADMOR, *Convergence of Spectral Methods for Hyperbolic Initial-Boundary Value Systems*, SIAM J. Numer. Anal. **24**(1987), pp. 532-537.

[38] D. GOTTLIEB AND S. A. ORSZAG, *Numerical Analysis of Spectral Methods: Theory and Applications.* CBMS-NSF **26**. SIAM, Philadelphia, 1977.

[39] D. GOTTLIEB, S. A. ORSZAG, AND E. TURKEL, *Stability of Pseudospectral and Finite-Difference Methods for Variable Coefficient Problems*, Math. Comp. **37**(1981), pp. 293-305.

[40] On the Convergence of the Fourier Approximation of Eigenvalues and Eigenfunctions of Discontinuous Problems (with M.S. Min) submitted to SINUM.

[41] D. GOTTLIEB AND C.W. SHU, *On the Gibbs Phenomenon V: Recovering Exponential Accuracy from Collocation Point Values of a Piecewise Analytic Function*, Numer. Math. **71**(1995), pp. 511-526.

[42] D. GOTTLIEB AND C.W. SHU, *On the Gibbs Phenomenon and its Resolution*, SIAM Review **39**(1997), pp. 644-668.

[43] D. GOTTLIEB AND C.W. SHU, *A General Theory for the Resolution of the Gibbs Phenomenon.* In TRICOMI'S IDEAS AND CONTEMPORARY APPLIED MATHEMATICS, National Italian Academy of Science, 1997.

[44] D. GOTTLIEB AND E. TADMOR, *Recovering Pointwise Values of Discontinuous Data with Spectral Accuracy.* In PROGRESS AND SUPERCOMPUTING IN COMPUTATIONAL FLUID DYNAMICS. Birkhäuser, Boston, 1984. pp. 357-375.

[45] S. Gottlieb and C.-W. Shu, *Total variation diminishing Runge-Kutta schemes*, Math. Comp., v67 (1998), pp.73-85.

[46] S. Gottlieb, C.-W. Shu and E. Tadmor, *Strong stability preserving high order time discretization methods*, SIAM Review, v43 (2001), pp.89-112.

[47] D. Gottlieb and C.E. Wassberg *Optimal Decomposition of the Domain in Spectral Methods for Wave Like Phenomenon* SISC Vol.22 no.2 (2000) pp. 617-632.

[48] F. Grasso and S. Pirozzoli, *Shock-wave-vortex interactions: Shock and vortex deformations, and sound production*, Theor. Comp. Fluid Dyn., v13 (2000), pp.421-456.

[49] F. Grasso and S. Pirozzoli, *Shock wave-thermal inhomogeneity interactions: Analysis and numerical simulations of sound generation*, Phys. Fluids, v12 (2000), pp.205-219.

[50] E. Harabetian, S. Osher and C.-W. Shu, *An Eulerian approach for vortex motion using a level set regularization procedure*, J. Comput. Phys., v127 (1996), pp.15-26.

[51] A. Harten, B. Engquist, S. Osher and S. Chakravarthy, *Uniformly high order essentially non-oscillatory schemes, III* J. Comput. Phys., v71 (1987), pp.231-303.

[52] J. S. HESTHAVEN, *A Stable Penalty Method for the Compressible Navier-Stokes Equations: II. One-Dimensional Domain Decomposition Schemes*, SIAM J. Sci. Comput. **18**(1997), pp. 658-685.

[53] J. S. Hesthaven, *On the Analysis and Construction of Perfectly Matched Layers for the Linearized Euler Equations*, J. Comput. Phys. **142**, pp. 129-147.

[54] J. S. HESTHAVEN, *Spectral Penalty Methods*, Appl. Numer. Math. **33**(2000), pp. 23-41.

[55] J. S. HESTHAVEN AND D. GOTTLIEB, *Stable Spectral Methods for Conservation Laws on Triangles with Unstructured Grids*, Comput. Methods Appl. Mech. Engin. **175**(1999), pp. 361-381.

[56] J. S. HESTHAVEN AND C. H. TENG, *Stable Spectral Methods on Tetrahedral Elements*, SIAM J. Sci. Comput. 2000 – to appear.

[57] D. GOTTLIEB AND C. E. WASBERG, *Optimal Strategy in Domain Decomposition Spectral Methods for Wave-Like Phenomena*, SIAM J. Sci. Comput. 1999 - to appear.

[58] J. S. HESTHAVEN, *A Stable Penalty Method for the Compressible Navier-Stokes Equations: III. Multidimensional Domain Decomposition Schemes*, SIAM J. Sci. Comput. **20**(1999), pp. 62-93.

[59] C. Hu and C.-W. Shu, *Weighted essentially non-oscillatory schemes on triangular meshes*, J. Comput. Phys., v150 (1999), pp.97-127.

[60] C. Hu and C.-W. Shu, *A discontinuous Galerkin finite element method for Hamilton-Jacobi equations*, SIAM J. Sci. Comput., v21 (1999), pp.666-690.

[61] M. Ivanov, G. Markelov, A. Kudryavtsev and S. Gimelshein, *Numerical analysis of shock wave reflection transition in steady flows*, AIAA J., v11 (1998), pp.2079-2086.

[62] J. Jerome and C.-W. Shu, *Transport effects and characteristic modes in the modeling and simulation of submicron devices*, IEEE Trans. Computer Aided Design of Integrated Circuits and Systems, v14 (1995), pp.917–923.

[63] G. Jiang and D.-P. Peng, *Weighted ENO schemes for Hamilton-Jacobi equations*, SIAM J. Sci. Comput., v21 (2000), pp.2126-2143.

[64] G. Jiang and C.-W. Shu, *Efficient implementation of weighted ENO schemes*, J. Comput. Phys., v126 (1996), pp.202-228.

[65] G. Jiang and C.-C. Wu, *A high order WENO finite difference scheme for the equations of ideal magnetohydrodynamics*, J. Comput. Phys., v150 (1999), pp.561-594.

[66] A. Kuo and L. Polvani, *Wave-vortex interaction in rotating shallow water. Part 1. One space dimension*, J. Fluid Mech., v394 (1999), pp.1-27.

[67] S. Lee, S. Lee and J. Yang, *Numerical solution of the system of Vlasov-Poisson equations*, J. Chin. Inst. Eng., v22 (1999), pp.341-350.

[68] D. Levy, G. Puppo and G. Russo, *Compact central WENO schemes for multidimensional conservation laws*, SIAM J. Sci. Comput., v22 (2000), pp.656-672.

[69] S. Liang and H. Chen, *Numerical simulation of underwater blast-wave focusing using a high-order scheme*, AIAA J., v37 (1999), pp.1010-1013.

[70] R. Liska and B. Wendroff, *Composite schemes for conservation laws*, SIAM J. Numer. Anal., v35 (1998), pp.2250-2271.

[71] R. Liska and B. Wendroff, *Two-dimensional shallow water equations by composite schemes*, Int. J. Numer. Meth. Fl., v30 (1999), pp.461-479.

[72] X-D. Liu, S. Osher and T. Chan, *Weighted essentially non-oscillatory schemes*, J. Comput. Phys., v115 (1994), pp.200-212.

[73] H. MA, *Chebyshev-Legendre Super Spectral Viscosity Method for Nonlinear Conservation Laws*, SIAM J. Numer. Anal. **35**(1998), pp. 869-892.

[74] H. MA, *Chebyshev-Legendre Spectral Viscosity Method for Nonlinear Conservation Laws*, SIAM J. Numer. Anal. **35**(1998), pp. 893-908.

[75] Y. MADAY AND E. TADMOR, *Analysis of the Spectral Vanishing Viscosity Method for Periodic Conservation Laws*, SIAM J. Numer. Anal. **26**(1989), pp. 854-870.

[76] Y. MADAY, S. M. OULD KAPER, AND E. TADMOR, *Legendre Pseudospectral Viscosity Method for Nonlinear Conservation Laws*, SIAM J. Numer. Anal. **30**(1993), pp. 321-342.

[77] A. MAJDA, J. MCDONOUGH, AND S. OSHER, *The Fourier Method for Nonsmooth Initial Data*, Math. Comp. **32**(1978), pp. 1041-1081.

[78] P. Montarnal and C.-W. Shu, *Real gas computation using an energy relaxation method and high order WENO schemes*, J. Comput. Phys., v148 (1999), pp.59-80.

[79] S. Osher and C.-W. Shu, *High-order essentially nonoscillatory schemes for Hamilton-Jacobi equations*, SIAM J. Numer. Anal., v28 (1991), pp.907–922.

[80] C.-W. Shu, *Total-Variation-Diminishing time discretizations*, SIAM J. Sci. Stat. Comput., v9 (1988), pp.1073-1084.

[81] C.-W. Shu, *Preface to the republication of "Uniform high order essentially non-oscillatory schemes, III," by Harten, Engquist, Osher, and Chakravarthy*, J. Comput. Phys., v131 (1997), pp.1-2.

[82] C.-W. Shu, *Essentially non-oscillatory and weighted essentially non-oscillatory schemes for hyperbolic conservation laws*, in *Advanced Numerical Approximation of Nonlinear Hyperbolic Equations*, B. Cockburn, C. Johnson, C.-W. Shu and E. Tadmor (Editor: A. Quarteroni), Lecture Notes in Mathematics, volume 1697, Springer, 1998, pp.325-432.

[83] C.-W. Shu, *High order ENO and WENO schemes for computational fluid dynamics*, in *High-Order Methods for Computational Physics*, T.J. Barth and H. Deconinck, editors, Lecture Notes in Computational Science and Engineering, volume 9, Springer, 1999, pp.439-582.

[84] C.-W. Shu and S. Osher, *Efficient implementation of essentially non-oscillatory shock capturing schemes*, J. Comput. Phys., v77 (1988), pp.439-471.

[85] C.-W. Shu and S. Osher, *Efficient implementation of essentially non-oscillatory shock capturing schemes. II*, J. Comput. Phys., v83 (1989), pp.32-78.

[86] C.-W. Shu, T.A. Zang, G. Erlebacher, D. Whitaker, and S. Osher, *High order ENO schemes applied to two- and three-dimensional compressible flow*, Appl. Numer. Math., v9 (1992), pp.45-71.

[87] C.-W. Shu and Y. Zeng, *High order essentially non-oscillatory scheme for viscoelasticity with fading memory*, Quarterly of Applied Mathematics, v55 (1997), pp.459-484.

[88] K. Siddiqi, B. Kimia and C.-W. Shu, *Geometric shock-capturing ENO schemes for subpixel interpolation, computation and curve evolution*, Graphical Models and Image Processing (CVGIP:GMIP), v59 (1997), pp.278-301.

[89] E. TADMOR, *The Exponential Accuracy of Fourier and Chebyshev Differencing Methods*, SIAM Review **23**(1986), pp. 1-10.

[90] E. TADMOR, *Stability Analysis of Finite-Difference, Pseudospectral, and Fourier-Galerkin Approximations for Time-Dependent Problems*, SIAM Review **29**(1987), pp. 525-555.

[91] E. TADMOR, *Convergence of Spectral Methods for Nonlinear Conservation Laws*, SIAM J. Numer. Anal. **26**(1989), pp. 30-44.

[92] A. Taflove (Ed.), **Advances in Computational Electrodynamics**. Artech House, Boston, 1998.

[93] L. VOZOVOI, M. ISRAELI, AND A. AVERBUCH, *Analysis and Application of Fourier-Gegenbauer Method to Stiff DIfferential Equations*, SIAM J. Numer. Anal. **33**(1996), pp. 1844-1863.

[94] L. VOZOVOI, A. WEILL AND M. ISRAELI, *Spectrally Accurate Solution of Nonperiodic Differential Equations by the Fourier-Gegenbauer Method*, SIAM J. Numer. Anal. **34**(1997), pp. 1451-1471.

[95] F. Walsteijn, *Robust numerical methods for 2D turbulence*, J. Comput. Phys., v114 (1994), pp.129–145.

[96] J. Yang, S. Yang, Y. Chen and C. Hsu, *Implicit weighted ENO schemes for the three-dimensional incompressible Navier-Stokes equations*, J. Comput. Phys., v146 (1998), pp.464-487.

[97] T. Zhou, Y. Li and C.-W. Shu, *Numerical comparison of WENO finite volume and Runge-Kutta discontinuous Galerkin methods*, submitted to Applied Numerical Mathematics.

[98] L. Jameson, *High Order Methods for Resolving Waves: Number of Points per Wavelength*, SIAM J. Sci. Comp. **15**, No. 4 (2000)

[99] R. D. Richtmyer, *Taylor Instability in shock acceleration of compreessible fluids*, Commun. Pure Applied Math, **23**, pp. 297-319, 1960

[100] E. E. Meshkov, *Instability of the interface of two gases accelerated by a shock wave*, Izv. Akad. Nauk. SSSR Mekh. Zhidk. Gaza **4**, pp. 101-104 (1969)

[101] A. N. Aleshin, E. I. Chebotareva, V. V. Krivets, E. V. Lazareva, S. V. Sergeev, S.N. Titov & S. G. Zaytsev *Investigation of Evolution of Interface After Its Interaction With Shock Waves*, Report No. 06-96, LANL.